MXene Enhanced Shape Memory Polymer Composites: The Rise of MXenes as Fillers for Stimuli-responsive Materials

Neha Bisht[1, #], Shubham Jaiswal[1,2, #], Jeet Vishwakarma[1,2], Sarvesh Kumar Gupta[1], Reuben J. Yeo[3], S. K. R. S. Sankaranarayanan[4,5], Chetna Dhand[1,2, *], Neeraj Dwivedi[1,2, *]

[1]CSIR-Advanced Materials and Processes Research Institute, Bhopal- 462026, India

[2]Academy of Scientific and Innovative Research (AcSIR), Ghaziabad- 201002, India

[3]Institute of Materials Research and Engineering (IMRE), Agency for Science, Technology and Research (A*STAR), 2 Fusionopolis Way, Innovis #08-03, Singapore 138634, Republic of Singapore

[4]Department of Mechanical and Industrial Engineering, University of Illinois at Chicago, Chicago, IL 60607, USA

[5]Center for Nanoscale Materials, Argonne National Laboratory, Argonne, IL 60439, USA

#Authors with equal contribution

*Corresponding Author

[*] **Email:** neeraj.dwivedi@ampri.res.in **and** neerajdwivedi6@gmail.com (N. Dwivedi)

chetna.dhand@ampri.res.in **and** chetnachem24@gmail.com (C. Dhand)

Abstract

Shape memory polymers (SMPs) are intelligent materials that can adopt a temporary form and then return to their original form in response to an external stimulus. They exhibit large deformation, good corrosion resistance, and are of lightweight and biocompatible. Nevertheless, SMPs suffer from low electrical and thermal conductivities and longer shape recovery times. To overcome these limitations, the search for suitable fillers is ever continuing. MXenes have emerged as promising layered material with exceptional functional and physicochemical characteristics, including excellent electronic, optical, mechanical, and thermal properties, with the additional benefit of the presence of functional groups. Although their application in SMPs is still in its early stages, MXenes have shown great potential as fillers for polymers. This review critically examines the integration of MXenes into SMPs, focusing on the mechanisms that enhance the overall properties of the SMP composite (SMPC). We discuss current research on MXene-enhanced SMPs and offer insights into how MXenes improve the electrical, thermal, and shape memory characteristics of polymers, leading to high-performance intelligent composites. Finally, we explore the applications of MXene-enhanced SMPs, gave the perspective on the potential of MXene and carbon-based materials as fillers, challenges in the technology, and future prospects.

Keywords: MXene, Shape memory polymer, Shape memory effect, Self-healing

1. Introduction

Shape memory polymers (SMPs) are a novel family of smart materials that can take a transient configuration and regain their original configuration upon exposure to an external signal [1]. This characteristic makes SMPs a versatile material amongst polymeric material systems. SMPs hold several advantageous features, including low density, lightweight, easy-processability, large deformation, corrosion-resistance, and actuation potential, distinguishing them from other stimuli-responsive materials, like shape memory ceramics and shape memory alloys (SMA). SMPs possess great potential in soft robotics, wearable electronics, electro/thermo-mechanical systems, biotechnology, and other essential applications. The shape memory effect (SME) is the predominant feature that enables SMPs to retain a temporary shape via their hard crystalline phase while allowing for a reversible recovery. While shape recovery can be achieved *via* multi-responsive modes, including electric field, pH, magnetic field, light energy, and so on, heat energy remains the most frequent method for achieving shape recovery. The temperature at or above which the shape recovery occurs is generally called as polymer glass transition temperature, T_g [2]. To employ these materials for practical applications, "programming" is the mandatory step, which includes the i) heating of the sample above T_g, ii) deformation of the sample for temporary shape, iii) cooling down of the sample to achieve the fixed temporary shape, and finally iv) heating of the sample above T_g to perform shape recovery and achieve the original shape. The materials may belong to multi-shape or two-way SMPs, depending on the number of forms to be acquired. Materials falling under the first type can memorize a variety of transient configurations and restore them in a very regulated, irreversible, one-way manner [3]. The second category includes materials that display programmed and reversible shape switching between two different shapes. However, SMPs have many significant drawbacks, such as low electrical and thermal conductivity, low tensile strength and stiffness, and slow actuation (or high shape recovery time), which restrict their potential commercial applications. One possible solution to these problems is to introduce one or more conductive fillers in the SMP matrix. Carbon-based fillers like carbon

nanotubes (CNTs), carbon nanofibers (CNFs), carbon dots (CDs), graphene, graphene oxide (GO), and reduced graphene oxide (rGO) can be introduced to improve the functional properties of SMPs [4-11]. For example, SMP composite was developed by Ha et al. by incorporating boron-doped single-walled CNTs (B-SWCNTs) into a polyurethane (PU) matrix, which exhibited superior mechanical, thermal, and electrical characteristics concerning pristine PU [12]. Du et al. enhanced the thermal, photo-thermal, and mechanical properties of SMPs by reinforcing functionalized graphene oxide (FGO) [13]. Zhang et al. successfully integrated oligomer-modified GO (omG) into a PU matrix, resulting in outstanding functional properties[14]. Yoo et al. incorporated poly(ε-caprolactone) (PCL) diol-modified NDs (f-NDs) into the PU matrix to enhance its shape recovery stress and mechanical characteristics[15].

In the quest to advance, miniaturize, and develop next-generation high-performance shape memory systems, the search for novel fillers for SMPs is ever continuing. Recently, MXenes, the emerging 2D transition metal carbides, nitrides, and/or carbo-nitrides having numerous reactive groups on their surface, have attracted considerable scientific and technological attention [16]. SMPs integrated with MXene exhibit enhanced properties due to MXene's high surface area [17], excellent electrical [18], and thermal conductivity [19], tailored surface chemistry [20], hydrophilicity [21], and biocompatibility [22]. The fundamental mechanism involves the dispersion of MXene nanosheets within the polymer matrix, forming a conductive network that significantly improves the material's responsiveness to external stimuli such as heat or electrical fields. Due to MXene’s excellent metallic conductivity, it facilitates uniform heat distribution within the polymer matrix, resulting in a faster shape recovery rate and recovery time of SMPs by reducing the energy barrier for molecular rearrangement. MXene also acts as a reinforcing agent, improving the stiffness and mechanical strength of SMPs [23] [24] [25]. The interaction between MXene nanosheets and the polymer chains at the molecular level helps in uniform stress distribution, reducing the risk of material fatigue and failure [26].

In this review, we critically discuss the rise of MXenes as fillers for polymers with a main focus on their role in regulating SMPs. Firstly, a brief overview of MXenes is presented, followed by a discussion on the fundamentals of the SME and the preparation methods for the SMP composites (SMPCs). Subsequently, the functional properties, such as thermal, electrical, mechanical, and self-healing characteristics with underlying fundamental mechanisms, are discussed. The article further presents the applications of MXene-enhanced SMPCs across various domains, including flame retardancy, actuation, energy storage, EMI shielding, and biomedical applications **(Figure 1)**. We have also provided a section that discusses the potential of MXene and carbon-based materials as fillers. Finally, we thoroughly discussed the challenges and future prospects of MXene-enhanced SMPCs in real-world applications.

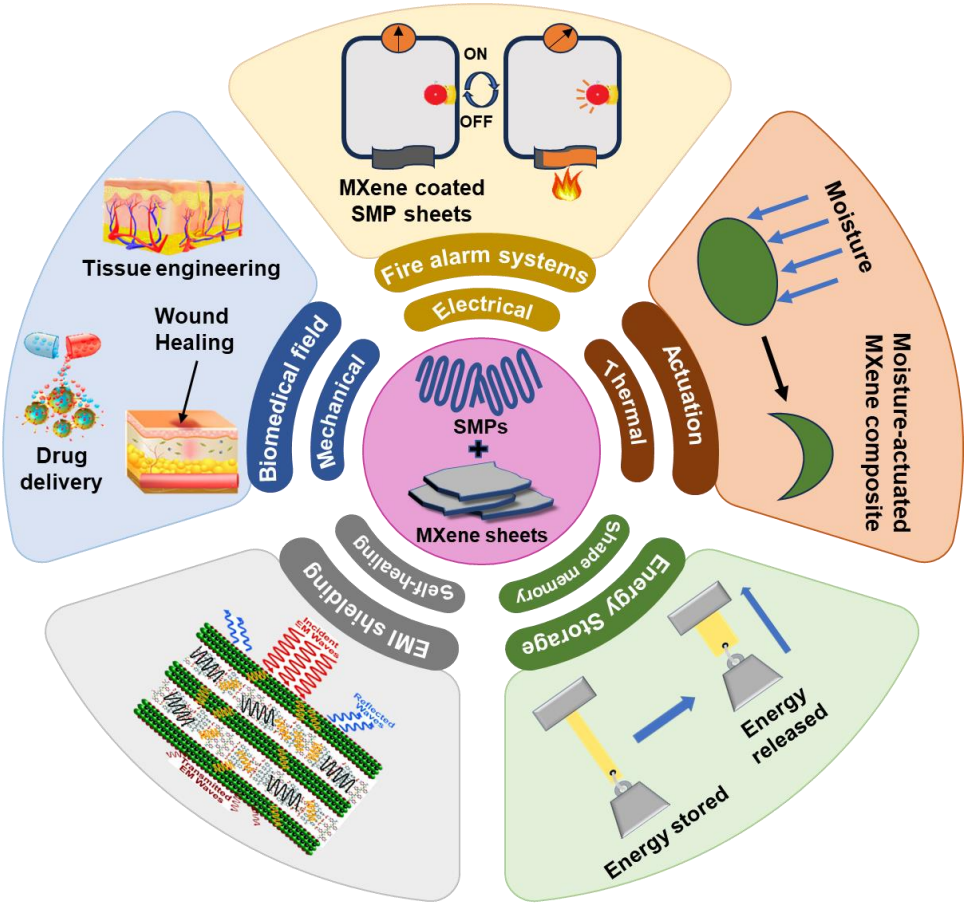

Figure 1. MXenes-enhanced shape memory polymers with their prospective applications.

2. MXenes

The discovery of graphene opened a new area to hunt for novel 2D materials with excellent functional and physicochemical properties [27-29]. A new class of novel 2D materials, including silicene, germanene, phosphorene, metal dichalcogenides, and metal oxides, have been discovered to show promising properties [30]. To meet the pace of technological advancement, the search for novel high-performance 2D materials is still continuing. Presently, the layered transition metal carbides and nitrides, called MXenes, that have a typical formula of $M_{n+1}X_nT_x$, where M and X represent transition metals and carbon and/or nitrogen, respectively, T_x shows functional groups such as O, OH, F, and/or Cl, attached to them, are at the center of research [31]. Potential MXene structures have increased to over 100 [32]. MXenes are made by the specific etching of A layer of its MAX phase precursor. The resultant material is then delaminated and exfoliated using ultrasonication to obtain the final product [33, 34]. The aqueous hydrofluoric acid (HF) or in-situ HF production by the interaction of (hydrochloric acid) HCl and lithium fluoride selectively removes the A-element layer(s) from the MAX phases.

$$M_{n+1}AlX_n + 3HF \rightarrow M_{n+1}X_n + AlF_3 + 1.5H_2$$

However, Huang et al. developed novel MAX phases and fluorine-free MXenes in 2019 using molten $ZnCl_2$ salt [35]. With this approach, researchers can now manufacture MXenes with chemicals that do not include or produce HF. The possibility of modifying the surface terminations of MXenes enriches their practical applications [36]. MXenes exhibit high electrical conductivity and fast electron kinetics, making them promising electrode materials for batteries [37] and electrochemical capacitors [38]. The excellent mechanical characteristics and surface functionalities make MXenes a promising reinforcement for polymers, ceramics, and metals to produce robust functional composites [39].

3. Shape Memory Effect in SMPs

Shape memory effect (SME) is a phenomenon that explains how SMPs can revert to their initial shape following a significant elastic deformation in response to a particular stimulus [40] [41]. The molecular

network of SMPs has switches that respond to an external stimulus. The network also contains net points that are connected via chain segments [1]. The chain segments deform elastically when paired with an appropriate/tailored programming stimulus. This distortion may be undone by reorienting the chain segments to restore the original structure or shape. The transition temperature (T_{trans}) (glass transition temperature (T_g)) facilitates the chain segment deformation, at which the network deforms elastically and can be fixed temporarily. The net points that decide polymer shape might alter according to chemical or physical processes, such as reversible covalent bonding or intermolecular interactions. An illustration of an SMP with thermal programming is shown in **Figure 2**. When heated over its transition temperature, T_{trans}; the material deforms into a soft rubber (or elastomer) due to the enhanced mobility of the molecular chains [42]. When cooled down to a temperature below T_{trans}, the deformation placed on the SMP will persist long after removing the external force. The original form is obtained by reheating the materials over the same T_{trans}.

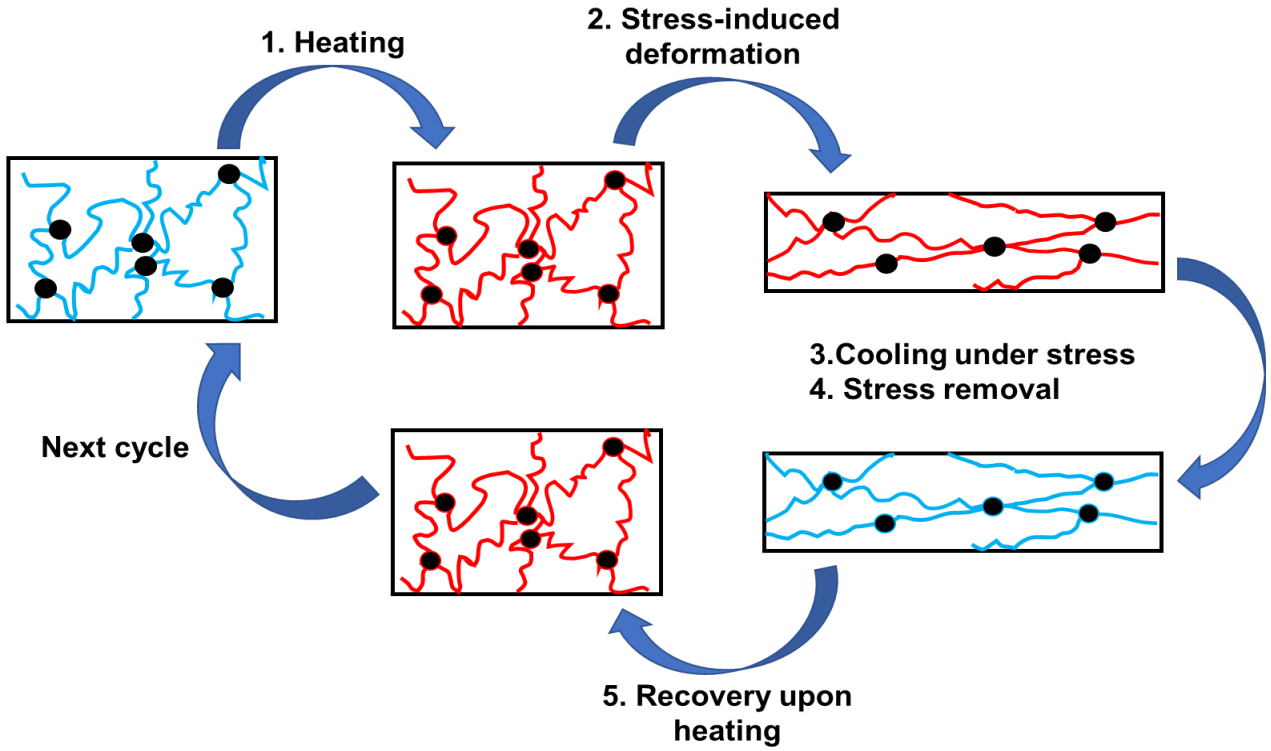

Figure 2. Thermally induced SME's molecular mechanism (black dots represent net points, blue lines represent elongated and fixed segments, and red lines represent relaxed segments).

Although SME was discovered in an AuCd alloy in 1932, it wasn't until 1971 that the attractiveness of this phenomenon became clear when considerable recoverable strain was observed in a NiTi alloy at the United States Naval Ordnance Laboratories [43] [44]. Many different types of solid, film, and even foam shape memory alloys (SMAs) are now easily fabricated. Only three of these alloy systems, those based on nickel-titanium (NiTi), copper (CuAlNi and CuZnAl), and iron (Fe), are currently of greater economic significance [44]. NiTi-based alloy systems have excellent biocompatibility and outstanding performance. Cu-based SMAs offer the benefits of cheap raw materials and good processing workability; among them, some even exhibit rubber-like properties after aging in martensite. Due to their highly affordable cost, Fe-based SMAs are promising for disposable fasteners or clamps. On the other hand, L. B. Vernon is credited for publishing the first article detailing SME in a US patent [45]. He described a dental material made of methacrylic acid ester resin that had "elastic memory" and could revert to its original shape when heated. However, SMPs, compared to SMAs, have gained immense interest because of their many versatile characteristics. Compared to SMAs, they provide deformation to a far higher degree (strain up to more than 200% for most of the materials) and a more extensive scope of variable mechanical characteristics, in addition to their inherent benefits of being affordable, lightweight, chemical inertness, corrosion resistant, and easily processable [46] [47].

4. Manufacturing Methods for MXene-enhanced SMPCs

There are a few primary methods for processing MXene-enhanced polymer composites: (i) Ex-situ blending (solution casting, compression molding, and vacuum-assisted filtration), (ii) in-situ polymerization, (iii) melt blending, and (iv) coating techniques.

4.1. Ex-situ blending

The properties of the fabricated composite materials depend on the bonding interactions among the polymers and MXene materials. Solution casting, which can be done on laboratory scales and uses colloidal Mxene, is the most popular way to make polymer composites [48]. In this technique, the

surface functionalized Mxene fillers and polymer matrices are mixed in a solvent that must then be extensively stirred to increase the homogeneity of the mixture [49]. After that, the mixture is poured into molds, and the solvent is evaporated to produce uniformly dispersed composite materials [50]. For instance, in order to achieve a composite with uniform dispersion, Li et al. ultrasonically mixed Mxene and polyvinyl alcohol (PVA) before being poured into a developed mold and placed to extract the solvent **(Figure 3A)** [51]. By using the solution casting process, Pan et al. reported the homogeneous dispersion of MXene in the PVA/MXene nanocomposites [52]. The same technique was also used to develop Ti_3C_2/ thermoplastic polyurethane (TPU) based SMPC that exhibited outstanding mechanical and thermal properties [53].

In some cases, the solution casting method can be further accompanied by a compression molding method in which the obtained composites are shaped in a desired manner by pressing at a high temperature [50]. For instance, using a homogenous combination of MXene and TPU modified with cationic modifiers in DMF, Yu et al. synthesized TPU/MXene SMPC by dispersing the mixture in water **(Figure 3B)** [54]. The developed composite materials that were molded by pressing at an elevated temperature showed uniform dispersion and flame retardancy. MXene may establish H-bonds with TPU chains when dispersed in solution, significantly enhancing the modified MXene's dispersion. Ma et al. crafted a nanocomposite, SiCnw/MXene/PVDF, by synthesizing SiCnw/MXene within a PVDF matrix through a process involving electrostatic self-assembly, solution casting, and hot pressing[55]. The SiCnw inhibited the aggregation of MXene nanosheets and their effective interconnectivity, resulting in their homogeneous dispersion in the PVDF matrix. This PVDF/SiCnw/MXene nanocomposite improved the impedance matching and polarization loss while tuning the ohmic loss, resulting in a superior Electromagnetic (EM) absorption performance. In another report, Rajavel et al. synthesized MXene/PVDF composite in ethanol, followed by ultrasonication [56]. The mixture underwent heating to remove the ethanol, and then hot pressing was used to generate the PVDF composite materials. In vacuum-assisted filtration, MXene and the polymer are mixed into

the solvent to achieve a uniformly dispersed solution. Using a filter membrane, the solute and solvent particles are separated under vacuum [57]. Liu et al. mixed $Ti_3C_2T_x$ MXene with waterborne PU in water to develop highly ordered nano-films **(Figure 3C)** [58]. The hydrogen bond interactions between MXene and PU enhanced the films' toughness and EMI shielding effectiveness.

4.2. In-situ polymerization

In the in-situ polymerization method, the polymer precursor is combined with MXene nanofillers and subsequently polymerizes to produce macromolecules under certain circumstances [59]. The fact that the polymer chains develop close to the nanofiller's surfaces is the main benefit of this strategy. The first step of the process is assembling the monomers on the surface of MXene via intermolecular interactions. Then, the polymerization of the monomers is done with the help of various techniques [60]. This method can effectively enhance the MXene interlayer spacing and cause MXene to be dispersed uniformly throughout the polymer matrix. Utilizing this concept, PANI@TiO_2/$Ti_3C_2T_x$ composite was fabricated and obtained by converting $Ti_3C_2T_x$ to TiO_2, after which the monomers of aniline were assembled on the MXene surface. The polymerization of aniline into PANI was done with the help of the initiator, APS [61]. The capacitance of the developed PANI@TiO_2/$Ti_3C_2T_x$ composite was twice than that of pure MXene. Zhang et al. also fabricated Ti_3C_2/PAM hydrogels that showed outstanding mechanical strength and enhanced drug delivery capability **(Figure 3D)** [62]. Tong et al. developed a sandwich-shaped PPy/$Ti_3C_2T_x$ composite film electrode using in-situ electrochemical polymerization. The prepared composite film exhibited good electrical capacitance, and due to the interaction of a bigger surface area and better conductivity, the produced composite film displayed good electrical capacitance and efficient ion transport pathways for fast energy storage because of the synergism of large surface area and better conductivity **(Figure 3E)** [63]. In another report, CNF/$Ti_3C_2T_x$ aerogels (CTA) were developed using the Hydrogen bonding interactions between cellulose nanofibers (CNF) and MXene [64], after which they were thermally annealed and incorporated in Epoxy with vacuum assistance **(Figure 3F).** The developed 3D EP nanocomposites

demonstrated outstanding EMI shielding efficiency and percolation threshold. In another report, via vacuum-assisted impregnation and curing technique, MXene/EP composites were prepared that exhibited good EMI SE and mechanical characteristics [65]. Like many traditional polymers, the MXene-SMP polymer composites can also be developed through in-situ polymerization, which can have the additional advantage of the more interactive nature of MXenes with polymer matrix.

4.3. Melt blending

In the melt blending method, MXene is incorporated into the polymer matrix by heating the polymer above its melting point. However, this method only applies to polymers that can be treated by melting, such as thermoplastics [50]. Zhang et al. used a high-speed mixer to combine ultrahigh molecular weight polyethylene (UHMWPE) powder with Ti_3C_2 nanosheets, and the obtained nanocomposites showed outstanding tensile and breaking strengths [66]. Shi et al. developed nanocomposites of $Ti_3C_2T_x$ and polypropylene (PP) using the melt blending technique [67]. Sheng et al. combined MXene and TPU in a torque rheometer, stirred the mixture for 6 minutes at 180 °C and 60 rpm, and then compressed the sample to get the required shape **(Figure 3G)** [68]. The prepared composite displayed excellent mechanical and thermal properties.

4.4. Coating techniques

Polymers and MXenes can also be mixed effectively by using the coating method. For instance, by dipping, Lin and co-workers coated MXene onto the surface of flexible polyurethane foam (FPUF), that significantly decreased the FPUF's flammability and smoke emissions[69]. A novel UV-curable nanocomposite coating, comprising intumescent flame-retardant (IFR) and MXene nanosheets, was created by introducing surface-modified MXene sheets into the IFR coating framework. This was then applied to rigid polyurethane (RPU) foam surfaces to produce coated RPU foams using a spray-coating and UV-curing technique [70]. Using a dip-coating method, the positively charged chitosan (CS) was wrapped around the negatively charged MXene on the PU foam's core (MXene@CS@PU) **(Figure 3H)** [71]. The coating can bear over 5000 cycles of compression release, with a response time of just

19 ms. PPy-functionalized Ti_3C_2 was dip-coated onto poly(ethylene terephthalate) (PET) surfaces to provide conductive surfaces for EMI shielding applications [72].

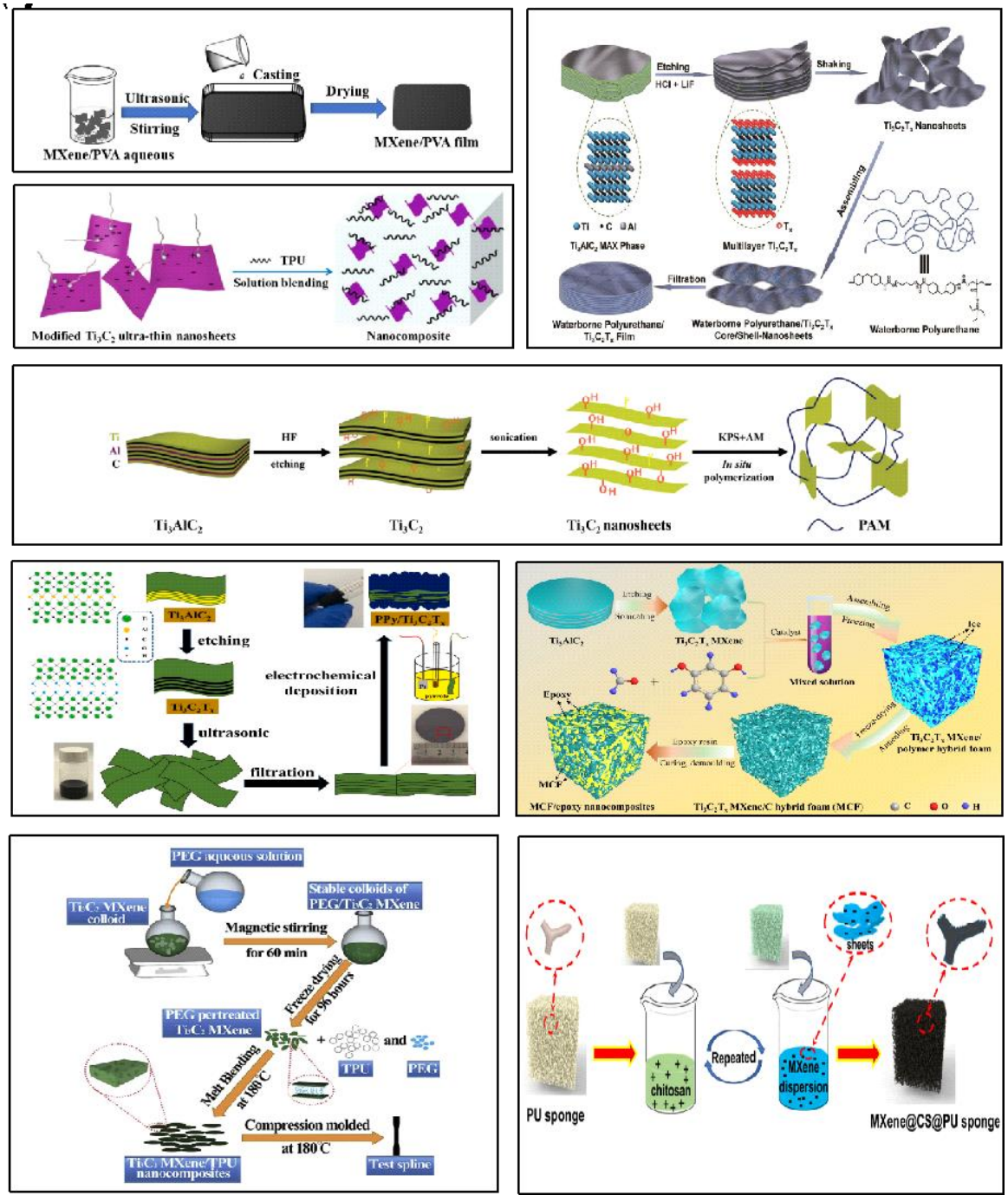

Figure 3. (A) Preparation of PVA/MXene film [51]. **(B)** Fabrication of TPU/modified Ti_3C_2 nanocomposites via solution blending [54]. **(C)** Preparation of polyurethane/$Ti_3C_2T_x$ MXene nacre-like nanocomposite film [58]. **(D)** Ti_3C_2/PAM hydrogels are fabricated by in-situ free radical polymerization with Ti_3C_2 nanosheets as a crosslinker [62]. **(E)** Preparation of PPy/$Ti_3C_2T_x$ films [63]. **(F)** Fabrication of TCTA/epoxy nanocomposites [64]. **(G)** Fabrication of TPU/MXene nanocomposites via melt blending [68]. **(H)** Preparation of MXene@CS@PU sponge via dip-coating method [71].

5. MXene enhanced SMPCs: Mechanisms and Properties

5.1 Mechanisms of MXene as a stimulus-responsive filler

MXenes, which include 2-D transition metal carbides, nitrides, and carbo-nitrides, have outstanding electrical and thermal conductivities, mechanical strength, and adjustable surface chemistry due to their terminal functional groups (-OH, -O, -F) [73, 74]. These characteristics make MXenes to be effective stimulus-responsive materials, considerably improving the electrical, thermal, and mechanical performance of SMPs. The terminal functional groups on the surface of MXenes allow for strong chemical interaction with the polymer matrix. These functional groups can establish hydrogen, ionic, and covalent interactions with the polymer chains, resulting in a strong interfacial interaction [75]. The presence of -OH and =O groups, for instance, promotes hydrogen bonding and increases the compatibility between MXene and hydrophilic polymer matrices [76]. Moreover, MXenes' hydrophilic behavior provides better interaction with polar polymeric matrices [77] [78], differently from other 2D materials, such as graphene. This improved interfacial adhesion facilitates effective stress transfer and better dispersion of the nanofillers within the SMP matrix [79] [25], leading to enhanced shape recovery rates and reduced recovery times [80] [81]. Furthermore, these functional groups can act as crosslinking sites, improving the elasticity and shape fixity of the SMPs. For example, the fluorine groups on MXene can introduce hydrophobic interactions, which might be beneficial for SMPs designed for environments where moisture resistance is crucial. Overall, the specific functional groups on MXene surfaces play a critical role in tailoring the properties of SMPs, making them highly tuneable for various advanced applications. This high interfacial adhesion assures that the MXenes are well incorporated into the SMP matrix, minimizing agglomeration and encouraging uniform dispersion throughout the material. This uniform dispersion is crucial because it guarantees that the MXenes are properly distributed, resulting in constant reinforcement throughout the composite [26]. When an external force acts on the composite, the strong interfacial interactions between the MXenes, with high aspect ratio [82], and SMP chains help to enhance this load transfer

process [83], thus eliminating localized stress concentrations that might lead to material failure. This produces a composite material with dramatically improved mechanical properties, including higher tensile strength [84], high breaking elongation, and flexibility [85]. Furthermore, MXenes have high electrical and thermal conductivity due to their elemental composition and unique structure. MXenes, when integrated into a polymer matrix, can create continuous conducting networks [81]. These networks are formed by the percolation of MXene nanosheets throughout the polymer, generating channels for electron and heat transport. This interconnected network significantly boosts the composite's conductivity and is crucial for electro-thermal actuation of SMPs [86]. MXenes' high conductivity enables that current or heat travels effectively through the composite, resulting in rapid and uniform heating. This uniform heating is critical for efficient shape recovery because it allows the whole polymer matrix to reach the activation temperature at the same time, allowing the SMP to return to its original shape quickly.

The next subsections cover new research on improving several aspects of SMPs, such as electrical, thermal, mechanical, self-healing, and shape memory capabilities, by incorporating MXene into the polymer matrix. We have attempted to give a complete review on MXene-enhanced SMPs based on existing studies. These studies investigate how MXene, with its unique combination of high conductivity, mechanical strength, and vast surface area, affects the performance of SMPs.

5.2. Properties of MXene enhanced SMPCs

5.2.1. Electrical Properties

MXenes span a broad spectrum of electrical characteristics, from metallicity and semi-conductivity to topological insulative. This is attributed to the broad array of surface functionalization possibilities, the ability to control variable thickness, and the substantial compositional variability [87]. MXenes demonstrate metallic conductivities characterized by high electron densities, resulting from strong coordination between the d electrons of the transition metals (denoted as 'M') and adjacent atoms [59].

Although MXenes such as Ti_2C, Ti_3C_2, Mo_2C, Mo_2C_2, and $Mo_2Ti_2C_3$ have been shown to have strong electrical properties, conductive insulation can be found only in some MXene-containing heavy transition metals (such as Cr, Mo) [88]. Surface terminations are essential in lowering the density of states (DOS), which shifts the transition metal "M"' d-band above the Fermi level and creates a band gap. This effect results from the hybridization of the "'M" d orbitals and the functional groups' p orbitals [89]. Further, low HF concentrations and short etching time also lead to an increase in the conductivity of MXenes as it results in lesser imperfections and large lateral sizes [90]. **Table 1** shows the electrical conductivity of various MXenes with the synthesis method.

Table 1. An overview of the several MXenes and their methods of production for electrical conductivity.

MXenes	Method of Synthesis	Electrical Conductivity (S/cm)	Ref.
$Ti_3C_2T_x$	"Evaporated-Nitrogen" Minimally Intensive Layer Delamination method	24000	[91]
Ti_3C_2	Hot press sintering	850	[92]
Ti_2CT_x	vacuum-assisted filtration method	1610	[93]
Nb_2CT_x		5	
V_2CT_x		998	
$Ti_3C_2T_x$		8570	
$Nb_4C_3T_x$		75	
Ti_3CNT_x		2712	
$Mo_2TiC_2T_x$		227	
Mo_2CT_x	vacuum-assisted filtration method	1.2	[94]
$Ti_3C_2T_x$	vacuum-assisted filtration method	2410	[95]

Polymers, on the other hand, are generally electrically insulating in nature. Adding MXenes to these polymers can enhance their electronic conductivity [49]. For instance, by incorporating varying

amounts of $Ti_3C_2T_x$ into epoxy (EP) resin, a notable enhancement in the electrical conductivity of the resulting EP/$Ti_3C_2T_x$ MXene composite was observed, reaching 4.52×10^{-4} S/m from the initial 10^{-16} S/cm conductivity of pure EP [96]. Similarly, Wang et al. fabricated a 3D $Ti_3C_2T_x$ MXene/C hybrid foam/epoxy nanocomposite (MCF/epoxy) [97]. They observed that as the MXene concentration in the mixture increases, the electrical conductivity of MCF-5/epoxy reaches to 184 S/m. Further, the 19.5 wt.% Ti_3C_2 MXene reinforcement in PVA enhances the conductivity of the composite upto 716 S/m, resulting in its improved EMI shielding properties [98].

The incorporation of MXene fillers into SMPs significantly enhances their electrical conductivity, leveraging the exceptional conductive properties of MXenes to improve the performance and functionality of these smart materials. For instance, Lu et al. synthesized a series of flexible and self-healable EMI shielding waterborne polyurethane (ADWPU) films by mechanically blending with $Ti_3C_2T_x$ (ADWPU-T). As MXene is known for its great metallic conductivity, it was seen that on increasing the content of $Ti_3C_2T_x$ in the ADWPU matrix from 3, 5, and 7 wt.%, the electrical conductivity of the composites increases four-fold **(Figure 4A)**, with observation of enhanced EMI SE [99]. Further, He et al. prepared the multifunctional PCM composites for electromagnetic interference (EMI) shielding functions by encasing poly(ethylene glycol) (PEG) into porous MXene/silver nanowire (AgNW) hybrid sponges by vacuum impregnation [100]. Melamine foams (MFs) were chosen as a template to coat with MXene/AgNW (MA) to create a continuous electrical/thermal conductive network (for reference, the obtained sponges (MFs) dipping in MA hybrid solution were named MF@MAx, where x represents the number of dipping times). Since the EMI shielding efficiency (SE) of EMI shielding materials is directly connected with their electrical conductivity, the conductivity of the sponges is measured **(Figure 4B)**. The electrical conductivity of MF@MA1/PEG was found to be 0.01 S/m due to the insufficient filler content within the sponge skeleton, which prevents the formation of an effective conductive network. This low conductivity indicates that the filler particles are too sparsely distributed to establish continuous pathways for electron transport. In

contrast, the electrical conductivities of MF@MA2/PEG and MF@MA3/PEG are significantly higher, measured at 23.71 S/m and 75.34 S/m, respectively. This dramatic increase is attributed to the presence of a 3D conductive network formed by the MA hybrid filler. In these composites, the higher filler content ensures that the conductive particles are closely packed and interconnected, enabling efficient electron flow throughout the material. The progressive enhancement in conductivity from MF@MA1/PEG to MF@MA3/PEG underscores the critical role of filler concentration in establishing robust conductive networks within polymer composites. In a recent work, Jaiswal et al. enhanced the electrical conductivity of SMPU by the reinforcement of Ti_3C_2 MXene as well as its Ti_3AlC_2 MAX phase precursor [101]. The enhancement of electrical conduction of SMPs upon MAX/MXene incorporation is ascribed to the presence of electrical conducting sites inside the polymer matrix as well as the conducting network, which facilitates electron movement/transfer across the sample. The enhanced electrical transport of SMP-composites due to the reinforcement of MXene could be crucial for electrically/thermally responsive shape memory applications.

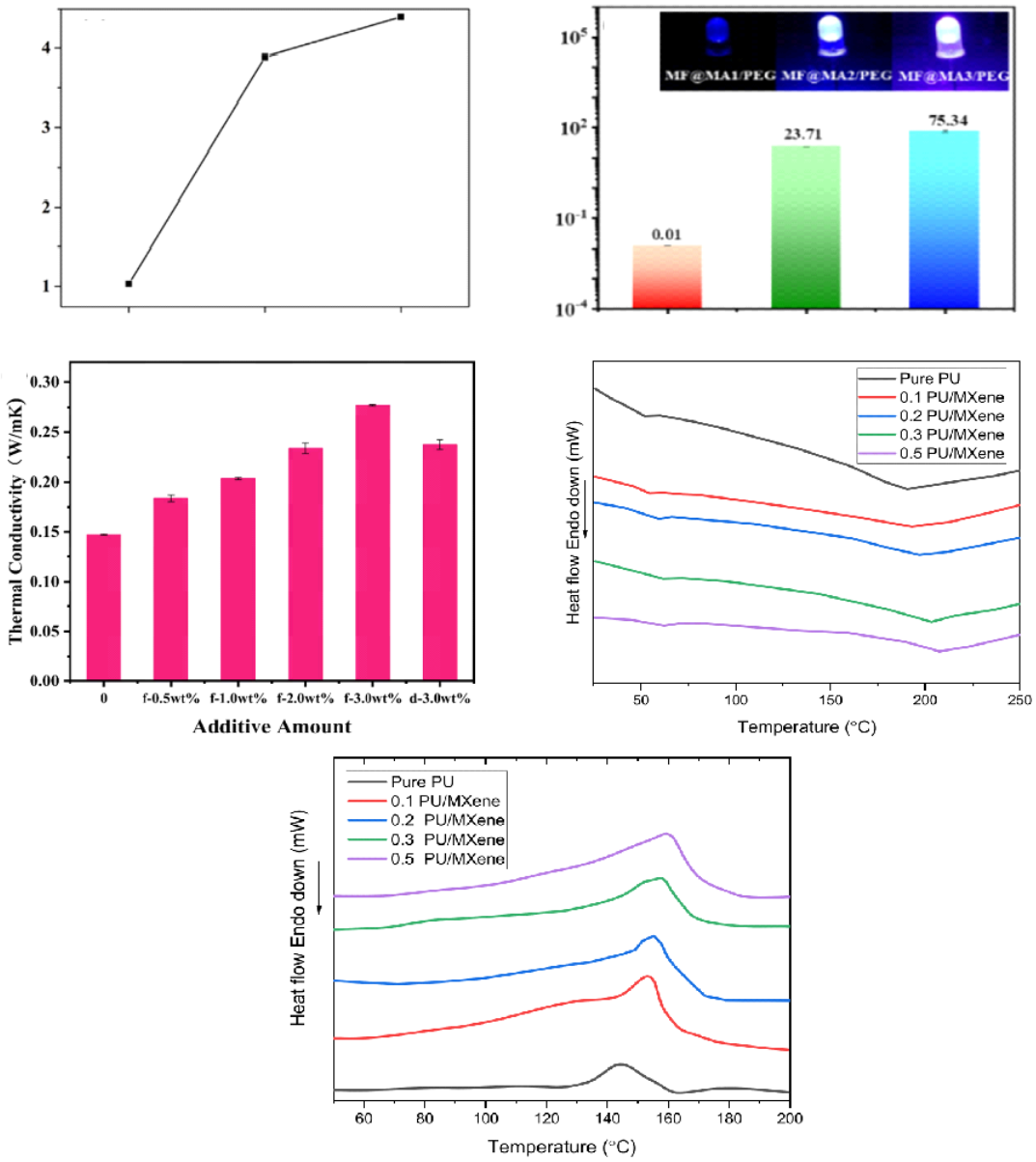

Figure 4. The electrical conductivity of **(A)** PU films [99]. **(B)** MF@MA/PEG [100]. **(C)** Thermal conductivities of pure TPU and its nanocomposites [102]. **(D)** Heating curve, and **(E)** Cooling curve of PU and PU/MXene (0.1-0.5 wt%) nanocomposites [80].

5.2.2. Thermal Properties

Thermal conductivity is the critical parameter for thermally triggered SMPs. Enhancing thermal conductivity improves heat dissipation (or thermal kinetics) and triggers the fast recovery in SMPs. Enhancement in heat dissipation is also essential for electronic gadgets as they become integrated and lightweight. Thanks to easy manufacturing, programmability, and significant deformation, SMPs are widely used in the aerospace, biomedical, sensor, and actuator industries. MXene possesses excellent

electrical conductance and good thermal conductivity. This is why polymers, initially heat insulators, can become conductive when reinforced with MXene [49]. MXene-based polymer hybrids [103] [104] have demonstrated somewhat improved thermal characteristics with fewer filler loadings compared to graphene-based nanocomposites [105] [106]. For instance, Kang et al. prepared Ti_3C_2/epoxy composites via solution blending [103]. The prepared composite increased thermal conductivity by 141.3% with 1 wt.% of Ti_3C_2 MXene fillers than that of neat epoxy. Wang et al. constructed a 3D-MXene/PDMS nanocomposite that increased its thermal conductivity by 220% with merely 0.7 wt.% of single-layer Ti_3C_2 [107]. Rajavel et al. developed MXene/PVDF nanocomposites with 22.55 vol.% Ti_3C_2, which shows thermal conductivity values four times higher than pure PVDF [56]. To speed up the heat transfer kinetics, the polymer and fillers must establish strong interactions promoting high thermal conductivity. When MXene concentrations are sufficient to form a network, its high thermal conductivity substantially surpasses the polymeric matrix's thermal resistance, resulting in homogeneous and high thermal conductivity. Higher thermal conductivity ensures the reliability and safety of batteries, capacitors, energy-storage devices, actuators, thermoelectric devices, EMI shielding materials, and aerospace materials by facilitating improved heat dissipation.

The poor thermal conductivity of SMPs demands high-performance fillers to improve the thermal-management capability for modern electronic applications where power densities are rising swiftly. MAX and MXene-based materials have also been introduced in the SMP matrix to engineer its thermal conductivity. For example, Jaiswal et al. observed a significant improvement in the thermal conductivity of SMPU with the addition of titanium carbide-based MAX and MXene [84]. This enhancement facilitated faster shape recovery in SMPU-MAX and SMPU-MXene composites. Measurements showed that pristine PU had a thermal conductivity of ~0.13 W/mK at room temperature (25 °C). In contrast, the addition of MAX and MXene improved thermal conductivity, even with low loadings of 0.25 wt%. For example, the thermal conductivity at 25 °C increased to ~0.21, 0.19, and 0.21 W/mK with the reinforcement of mixed Ti_2AlC+Ti_3AlC_2 MAX phase, Ti_3AlC_2

MAX phase, and Ti_3C_2 MXene, respectively. The presence of these fillers enhances heat transfer between molecular chains and reduces phonon scattering, thereby improving the thermal conductivity of PU composites. Moreover, Ti_3C_2 MXene nanosheets have attracted intensive attention due to their unique properties and have already been successfully applied in polymer composites for improved performance, such as thermal stability, and flame retardancy [108]. In this respect, He et al. incorporated poly(diallyldimethylammonium chloride) (PDDA) modified Ti_3C_2 (MXene) in thermoplastic polyurethane (TPU) matrix to reinforce fire safety and mechanical performance of TPU [102]. **Figure 4C** shows thermal conductivities of TPU and its nanocomposites. The thermal conductivities of the TPU composites increased with the addition of higher contents of additives. Specifically, when 3 wt% of functionalized Ti_3C_2 (f-Ti_3C_2) is incorporated into the TPU matrix, the thermal conductivity of the resulting TPU/f-Ti_3C_2-3.0 composite shows an 88.6% improvement compared to pure TPU. In contrast, under the same additive loading, the thermal conductivity of TPU/d-Ti3C2-3.0 (where d-Ti_3C_2 denotes a different form of Ti_3C_2) is not as high as that of TPU/f-Ti_3C_2-3.0. This discrepancy can be attributed to the presence of organic components in f-Ti_3C_2, which help preserve the structure of Ti_3C_2. These organic components prevent the Ti_3C_2 from being damaged and ensure its uniform dispersion within the TPU matrix, thereby enhancing the composite's thermal conductivity more effectively than d-Ti_3C_2. In a recent study, Sanaka et al. studied thermal properties of pure PU and PU/MXene (0.1-0.5 wt%) nanocomposites using heating and cooling curves [80] **(Figure 4D)**. It is observed that for pure PU, the T_m is 191 °C, which is increased to 193, 197, 203, and 207 °C for 0.1 PU/MXene, 0.2 PU/MXene, 0.3 PU/ MXene, and 0.5 wt% PU/MXene, respectively, indicating enhanced molecular alignment and ordering due to MXene. Cooling curves (**Figure 4E)** showed crystallization temperature (T_c) values followed pure PU < 0.1 PU/MXene < 0.2 PU/MXene < 0.3 PU/MXene < 0.5 wt% PU/MXene, with corresponding heat of crystallization (h_c) values reflecting MXene's nucleation effects and improved polymer packing during crystallization.

5.2.3. Shape Memory Properties

There are couple of important parameters that determine the material's ability to undergo SME and performance characteristics. The shape fixity ratio (R_f) and shape recovery ratio (R_r) are such crucial parameters that describe the shape memory capabilities of materials [109]. Most SMPs documented so far employ thermal energy as the principal stimulation. This situation's stimulation is the result of additional cross-links being thermally cleaved. Let us assume that these additional crosslinks are due to physical interactions. In this scenario, an additional differentiation can be made in T_{trans}, which includes a T_g and a melting temperature (T_m). The melting process is only possible within a very small temperature range, whereas glass transitions can happen at a wide range of temperatures. When the crosslinks consist of functional groups that undergo photo-reversible reactions using light as a stimulus, it extends the application of shape memory technology. Indirect heating of the material can be achieved by applying alternative stimuli like electric currents or electromagnetic fields. Shape memory properties are assessed by cyclic mechanical testing under various stimuli [110, 111]. Thermal or photomechanical testing techniques have been developed because the stimuli are primarily heat or light. In cyclic tests, parameters such as R_f, R_r, and switching temperature (T_{trans}) are measured, particularly under thermal stimulation. R_f evaluates the potential to maintain a mechanical deformation (ε_m) and create a temporary shape ε_u (N) over multiple cycles (N). The parameter R_r measures the ability to recover the permanent shape ε_p (N) after applying a particular deformation ε_m. It is calculated by comparing the difference in deformation observed during the SME (ε_m-ε_p) with the difference in deformation during the programming phase (ε_m-ε_p) of the previous cycle (N-1).

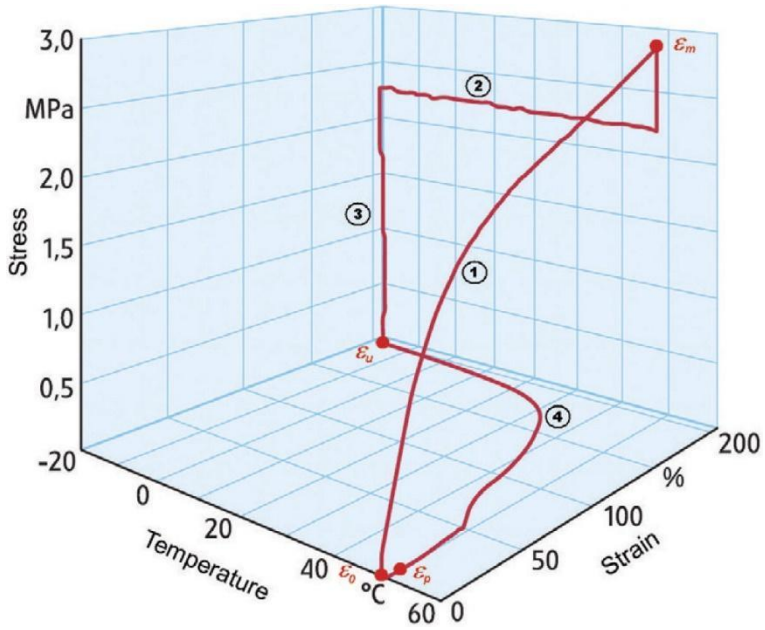

Figure 5. An example stress-strain-temperature curve (first cycle) for a thermoplastic SMP having a thermally actuated SME [112]. The experiment's first step controls strain, while steps two through four, up until the start of the following cycle, controls stress.

$$R_f(N) = \frac{\varepsilon_u(N)}{\varepsilon_m} \quad (1)$$

$$R_r(N) = \frac{\varepsilon_m - \varepsilon_u(N)}{\varepsilon_m - \varepsilon_u(N-1)} \quad (2)$$

Based on equations (1) and (2), it is clear that the optimal values for R_f and R_r should be 100%. Step 1 of an ordinary stress-controlled programming cycle involves clamping the sample in the tensile tester and stretching it to ε_m while keeping the molecular switch open. In thermally triggered shape memory materials, the molecular switches are activated by applying heat (T_{high}) above the transition temperature (T_{trans}). On the other hand, in light-induced shape memory materials, these switches are opened by exposing the material to irradiation at particular wavelengths λ, which leads to the breaking of the photosensitive links. To help the polymer chains relax, the stress is kept in place for a predetermined amount of time. The experiment then proceeds in a stress-controlled fashion. The temporary shape of the object is fixed by activating molecular switches (step 2) in the presence of a constant voltage σ. In thermally induced SMPs, the switches are closed through controlled cooling to temperatures below the transition temperature (T_{trans}). The switches are closed in light-induced SMPs

by irradiating them with appropriate wavelengths (λ). Then, the applied stress gradually decreases until stress equilibrium is reached at a pressure of 0 MPa (step 3) (**Figure 5**). The molecular switches are activated in the fourth step, maintaining a constant tensile stress of 0 MPa. This results in the shrinkage of the material and restoration of its permanent shape. Numerous theoretical concepts have been proposed to predict shape memory phenomena [113, 114]. These approaches rely on uniaxial deformation processes, each employing a distinct modeling methodology. The approaches mentioned above are derived from either mechanical modeling or thermodynamic perspectives. These methods make it easier to estimate temperature-dependent stress and strain, as well as stress and strain for deformed polymers.

Wang et al., for example, combined MXene and polyvinyl alcohol (PVA) to create a type of shape-programmable supermolecular nanocomposite film [115]. MXene acts as cross-linking points in the nanocomposite and provides extra intermolecular hydrogen bond contact between PVA in this film, giving it a strong shape-fixing feature. It should be noted that pure PVA has no water-responsive SME. However, it was reported that all of the samples exhibited high R_f and R_r (both >90%), indicating that the incorporation of MXene into PVA improved its water-responsive SME. In another report, The effects of MXene@PANI on the ability of epoxy (EP) resin coatings to self-heal were discussed by Dong et al [116]. NIR imaging revealed that the EP coating is unable to repair itself after being scratched. However, the addition of MXene to the MXene/EP coating caused the scratched area to shrink from 95 μm to 12 μm due to the photothermal conversion action of MXene, increasing the self-healing efficiency to 88%. Additionally, the MXene@PANI/EP coating improved the self-healing efficiency by 91%, resulting in a reduction in scratch size from 113 μm to 10 μm. In a recent study, Zhang et al. developed a flame-resistant paper using SMPU/MXene, which demonstrated exceptional fire retardancy and quick self-extinguishing capabilities [117]. Unlike the pristine SMPU paper, the SMPU/MXene paper maintained its shape without melting or dripping during combustion. The paper can self-unfold when heat-stimulated, taking 10 s to recover to its original shape after being folded,

which is faster than SMPU paper due to the presence of nanofillers **(Figure 6A)**. The SMPU/MXene paper exhibited excellent shape memory properties, remaining smooth without creases, and the MXene layer stayed intact. As electrically-stimulated, MXene coating effectively activated the SMPU paper by producing heat, which facilitated shape recovery **(Figure 6B)**. The temperature increased uniformly except at the edges, reaching 37.8 °C, which is sufficient to trigger shape memory behavior. Though the recovery process took about 60 s and was not completely flat, the paper's minor shape changes can be used to protect circuits through self-cutting performance. Further, McLellan et al. also highlight the significant role of MXene in enhancing the shape memory behavior of TPU/PLA shape memory composites [118]. According to their findings, the most favourable shape memory outcomes for the TPU/PLA composite are achieved when incorporating 2 wt% of MXene. This incorporation results in notable improvements in both actuation speed and recovery ratio. Specifically, the composite with 2 wt% MXene can rebound to 90.4% of its initial shape in just 13.8 s. In comparison, a composite without MXene (0 wt%) only recovers to 78.9% of its original shape in approximately 26 s **(Figure 6C)**. The enhanced recovery is attributed to the structural changes induced by the high MXene content. The presence of MXene leads to a more consistent TPU phase, which is crucial since TPU serves as the recuperating element responsible for restoring the material to its permanent state. The introduction of 2 wt% MXene plays a pivotal role in connecting adjacent TPU spheres, establishing a more robust and uninterrupted phase. This improved structure significantly enhances the material's capacity for swift and complete recovery, demonstrating the effectiveness of MXene in optimizing the shape memory properties of TPU/PLA composites. In another study, the researchers explored shape reconfiguration in actuators made from a combination of MXene and poly(vinyl alcohol) (PVA) [119]. This was achieved by leveraging the unique functional (F) groups on the surface of MXene, which interact with the hydroxyl groups in the PVA chain. This interaction forms a reversible "lock" structure, enabling the actuator to change its shape effectively. The team investigated two types of SMEs in the actuator: those triggered by NIR light and those triggered by thermal changes. They found that the R_r and R_f

improved with higher NIR light intensity. **Figure 6D** illustrates this relationship, showing that at lower NIR intensities (0.02 W/cm^2, 0.04 W/cm^2, and 0.06 W/cm^2), the actuator's SME was not satisfactory, with R_r values below 90%. However, at higher intensities (0.08 W/cm^2 and 0.10 W/cm^2), the R_r values exceeded 90%. Additionally, the actuator demonstrated a temperature-dependent SME, as shown in **Figure 6E**. The SME improved progressively with increasing temperature within a specific range (50-90 °C). At temperatures of 80 °C and 90 °C, the actuator's performance was particularly impressive, with both the R_f and R_r values exceeding 90%. This study highlights the potential of MXene/PVA-based actuators for applications requiring precise and responsive shape changes, driven by either light or heat. Recently, Guo et al. developed a high-performance multi-stimuli-responsive shape-memory and self-healing composite film by embedding MXene nanosheets into a sodium carboxymethyl cellulose (CMC) and PVA matrix [120]. The MXene nanosheets enhance the film's mechanical strength and provide efficient solar-thermal conversion for robust light-actuated shape-memory properties. The composite showed exceptional shape-memory response to heat, light, and water. In the heat-triggered shape recovery process, the shape-memory mechanism relies on PVA crystalline domains and hydrogen bonds for temporary shape fixation, with the amorphous CMC and PVA providing elasticity for shape recovery **(Figure 6F)**. MXene nanosheets act as cross-linking points, increasing the stationary phase ratio and speeding up recovery. NIR light-induced shape recovery mimics the thermal process, where photothermal MXene nanosheets generate heat to melt the reversible phase, thus restoring the temporary shape **(Figure 6G)**. Water-induced shape recovery works by lowering the T_g, expanding the composite network, and decreasing resistance to molecular chain movement, releasing the temporary shape when T_g drops below ambient temperature, enabling shape recovery **(Figure 6H)**.

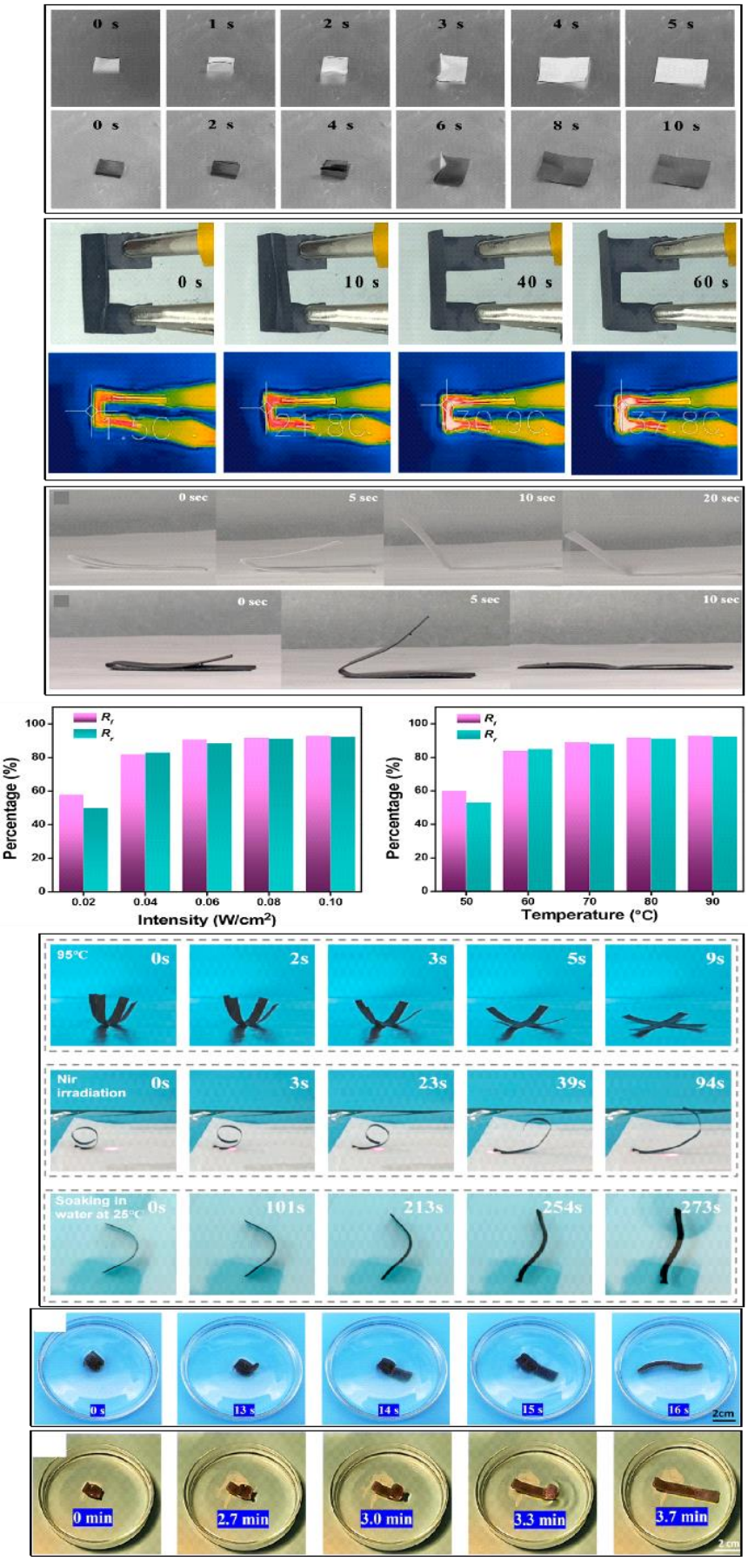
0 s
1 s
2 s
3 s
4 s
5 s
0 s
2 s
4 s
6 s
8 s
10 s
0 s
10 s
40 s
60 s
0 sec
5 sec
10 sec
20 sec
0 sec
5 sec
10 sec
Percentage (%)
Intensity (W/cm²)
Temperature (°C)
95°C
0s
2s
3s
5s
9s
Nir irradiation
0s
3s
23s
39s
94s
Soaking in water at 25°C
0s
101s
213s
254s
273s
0 s
13 s
14 s
15 s
16 s
2cm
0 min
2.7 min
3.0 min
3.3 min
3.7 min

Figure 6. (A) The process of shape recovery of folded-up **(a)** SMPU paper and **(b)** SMPU/MXene paper on the hot plate of 60 °C [117]. **(B)** The optical and infrared snapshots of electro-triggered shape memory behavior of SMPU/MXene paper [117]. **(C)** Shape memory performance of **(a)** 0 wt % MXene activation images at 0, 5,10, and 20 s; **(b)** 2 wt % MXene composite activation images at 0, 5, and 10 s [118]. SME of the MXene-based soft actuator at different **(D)** NIR light intensities, **(E)** temperatures [119]. Recovery process of CP3@M2: **(F)** petal shape at 95 °C, **(G)** spring shape under NIR irradiation, and **(H)** U shape in water at 25 °C [120]. Shape recovery of MXene based shape memory hydrogel at different time intervals **(I)** under 60 °C**,** and **(J)** NIR irradiation [121].

Recently, Hu et al. have created a MXene-based shape memory hydrogel for the development of wound-dressing hydrogels intended to repair skin by combining MXene, gelatin, poly(ethylene glycol) diacrylate (PEGDA), and N,N′-methylenebis(acrylamide) (HEAA) [121]. The first network layer was established by crosslinking HEAA and PEGDA, while the second layer was made by hydrogen bonding between MXene, PHEAA, and gelatin. This hydrogel exhibited improved mechanical properties and thermally induced shape memory attributes. Compared to hydrogels without MXene, the MXene-based hydrogel showed considerably higher Young's modulus, tensile strength, and elongation at break up to a particular threshold. The hydrogel could restore its former shape after 16 s when submerged in water **(Figure 6I)**, or in a few minutes under light irradiation **(Figure 6J)**. **Table 2** presents the comparison of various MXene enhanced SMPCs with other SMPCs in terms of their enhanced shape memory performance.

Table 2. Comparison of MXene enhanced SMPCs properties with other SMPCs.

S.No	**Shape memory polymer composites**	**Stimulus**	**Shape fixity ratio (Rf) (%)**	**Shape recovery ratio (Rr) (%)**	**Recovery time (s)**	**Ref.**
1	CMC/PVA@MXene	heat/NIR light/water	68.33	99.35	13	[120]
2	PCL/TPU/CNTs	heat	96	94	76	[122]

3	nHA/PU	heat	>90	>90	10	[123]
4	PHB/PCL/CNFs	heat	100	>95	125	[124]
5	MXene/PVA	heat/NIR light	>90	>90	-	[119]
6	MXene/TPU/PLA	heat	-	90.4	13.8	[118]
7	MXene/PVA film	water	>90	>90	-	[115]
8	PLA-MXene	heat	-	100	60	[26]
9	MF@MA/ PEG	NIR light	100	100	-	[125]
10	HPU−AH−rGO	heat/sunlight/micro wave	-	97.1	21	[126]

5.2.4. Self-healing properties

During shipping and use, organic coatings inevitably degrade, diminishing their barrier effectiveness and contributing to the corrosion of the underlying metal. Hence, the ability of coatings to self-heal becomes paramount, enhancing protection and prolonging their service life. Various self-healing coating approaches are under investigation, utilizing both autonomous and non-autonomous healing mechanisms [127]. The autonomous approach involves infusing coatings with healing agents and corrosion inhibitors, enabling them to restore protective properties. However, achieving lasting healing necessitates high levels of fillers and inhibitors. On the other hand, non-autonomous healing relies on SMPs to revive the polymer matrix's chemical bonds and physical structure, thereby enhancing protection. SMP-based self-healing coatings excel in repairing damaged areas due to their remarkable SME triggered by thermal or light stimulus. By reacting to light stimulation as pigments, adding photothermal agents to these coatings can further stimulate the mobility in the molecular chains and the polymer matrix interlocking. These agents can harness light energy, converting it into heat energy upon light exposure. MXene has received much interest as a photothermal agent because of its strong photothermal conversion capability and exceptional TC. In a report by Dong et al., MXene@PANI

composites were synthesized via chemical oxidation and used it as a photothermal agent to induce SME of the epoxy resin **(Figure 7A)** [127]. The incorporation of MXene@PANI (5 wt.%) into the epoxy resin not only improved its protective properties but also demonstrated an impressive 91% self-healing efficiency. In recent studies, Gao et al. prepared a flame-retardant composite phase change material (CPCM) comprising olefin block copolymer (OBC), paraffin (PA), and MXene (PA/OBC/MXene) for secure thermal management (**Figure 7B**) [83]. This CPCM displayed an impressive self-healing of 89.60% and exhibited thermal or light-driven shape memory properties. Further, Hu et al. also manufactured waterborne polyurethane (WPU)/MXene aerogel that showed outstanding photo-actuated self-healing and shape memory properties, with a dimension retention of 98% at 70 °C [128]. The light-actuated self-healing efficiency of WPU@MXene3/PEG reaches 82.9%. **Figure 7C** depicts how the crack in the sample entirely vanishes following light irradiation. The self-healing effect is caused by the wetting, diffusion, and re-entanglement of PEG melts and WPU soft segments. MXene nanosheets absorb light, convert it to heat, and transport that heat to PCMs, elevating the interior temperature to PEG melting point. When the temperature reaches the soft segment's T_m, the WPU segments at the fracture disperse and re-entangle, thereby healing the break. After the NIR light is withdrawn, PEG crystallizes, bridging the crack and effectively affixing the fractured parts. Similarly, Lu et al. performed a study in which they created superior EMI shielding and self-healing films using castor oil-derived WPU [99]. The addition of 2-aminophenyl disulfide accelerated the post-chain-extending process, which was unique to their technique. This method resulted in considerable improvements to the mechanical and functional qualities of WPU films. $Ti_3C_2T_x$ nanosheets were well dispersed inside WPU emulsions, which was critical to their effectiveness. This dispersion occurred without precipitation and remained stable for more than four months. The mechanical characteristics of the films improved significantly after post-chain extension and $Ti_3C_2T_x$ nanosheet integration. The sheets' tensile strength increased to a remarkable 15 MPa. Additionally, the films retained excellent self-healing capabilities, able to heal at 60 °C within just 5 min. This rapid self-healing is attributed to

the disulfide exchange mechanism inherent in the material. Moreover, the films exhibited notable shape memory performance, even at a relatively low elongation at break of approximately 30%. Recently, Guo et al. developed an efficient, multi-stimuli-responsive composite film (CMC/PVA@MXene) with shape memory and self-healing characteristics [120]. These composite films exhibited amazing self-healing properties, which were initiated by just moistening the scratched surface. **Figure 7D** depicts SEM images of CP3@M3 both before and after the self-healing process (for reference, films are identified as CPX@MY, where X is the mass ratio of PVA to CMC and Y is the mass fraction of MXene relative to the CMC/PVA matrix). Moistening the scratched surface reduced its width from 59.6 to 8.5 μm. In particular, moisture-treated parts had a much lower fracture width than untreated ones.

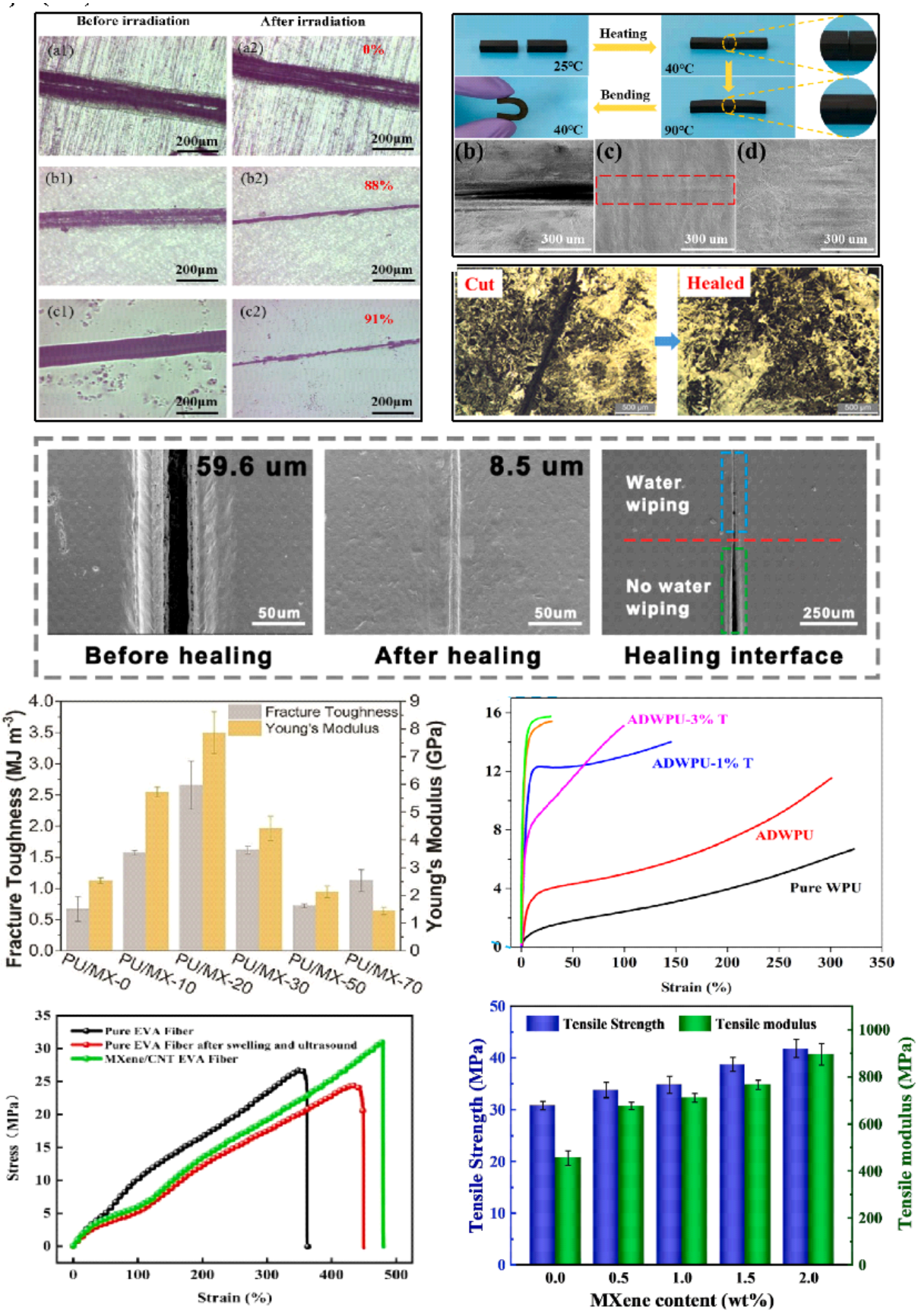

Figure 7. (A) Optical images of sctrach mark before and post-NIR light exposure for (a1-a2) EP, (b1-b2) MXene/EP, and (c1-c2) MXene@PANI/EP [127]. **(B)** (a) Self-healing performance of PA/OBC/ MXene CPCM. SEM pictures of (b) the cut PA/OBC/ MXene CPCM, (c) the surface of PA/OBC/

MXene CPCM, and (d) the interior of the healed PA/OBC/ MXene CPCM sample [83]. **(C)** POM images for fractured cut sample and self-healed sample [128]. **(D)** Surface scratch self-healing process of CP3@M3 [120]. **(E)** Fracture toughness and Young's modulus of PU/MX samples [58]. **(F)** Stress-strain curves for composite films with various content of $Ti_3C_2T_x$ flakes [129]. **(G)** Stress-strain curves of pure EVA fiber, pure EVA fiber after swelling-ultrasonic treatment, and MXene/CNTs/EVA fiber [85]. **(H)** Tensile strength and tensile modulus of WEP and MXene/WEP nanocomposites [25].

5.2.5. Mechanical properties

MXenes with versatile composition and various surface terminates (-O, -F, and -OH) attracts huge attention for mechanical applications. In composite materials, the inclusion of $Ti_3C_2T_x$, a type of MXene, holds great promise due to its unique functional groups present on the surface and high surface area [130]. By strengthening the connection between the polymer matrix and filler, these functional groups on $Ti_3C_2T_x$ improve the material's overall mechanical properties. The interactions among individual nanoflakes within Ti_3C_2 macro-films also significantly impact their mechanical behavior [131]. Xie et al. demonstrated that MXene/CNTs/EVA fibers had excellent mechanical characteristics and deformability, making them perfect for wearable electrical devices [85]. They created a strain sensor utilizing a swelling ultrasonic approach, leveraging the unique strain-related microcrack structure formed by the interaction of $Ti_3C_2T_x$ (MXene) and CNTs, as well as the shape memory feature of ethylene vinyl acetate polymer (EVA). The MXene/CNTs/EVA fiber can be stretched, bent, and twisted without breaking, demonstrating outstanding deformability. The MXene/CNTs/EVA fiber exhibits higher elongation at break than pristine EVA fibre, but lower tensile strength at smaller strains (< 380%) (**Figure 7F)**. Tests found that swelling and ultrasonic treatments reduced the tensile strength of EVA fibre while increasing elongation at break. Adding 1D CNTs and 2D MXene improved the breaking elongation and strength of the MXene/CNTs/EVA fiber, ensuring its suitability for wearable electronics. Moreover, Chi et al. have recently introduced MXene/WE SMPCs, which displayed enhanced mechanical properties, thermo-mechanical cycle stability, and resistance to creep, all while preserving exceptional shape memory capabilities [25]. **Figure 7G** illustrates the tensile strength, and modulus of WEP and its nanocomposites. The data reveal that as the content of MXene nanosheets

increased, the tensile strength and modulus of the nanocomposites improved progressively. Specifically, the tensile strength and modulus of the 2 wt% MXene/WEP nanocomposites rose by 40% and 94%, respectively, compared to the pristine WEP, reaching 42 MPa and 749 MPa. This enhancement is due to the effective dispersion of MXene and the strong interfacial interactions between MXene and the WEP matrix, which reduce stress concentration and slow down crack propagation, thereby requiring more energy to fracture the nanocomposite.

6. Applications of MXene-Shape Memory Polymer Composites

6.1. Fire alarm sensor/ Flame retardancy/Fire monitoring

MXene belongs to a novel class of 2D materials with intrinsic strong metallic conductivity, superior mechanical stability, and outstanding thermal stability. MXene's distinct 2D structure makes it an effective physical barrier that helps polymers to withstand fire [117]. Furthermore, it appears from the research results that TiO_2 nanoparticles are produced on MXene's surface during burning. These nanoparticles acts as a catalyst that effectively reduces the concentration of hazardous gases and smoke [132] [117]. However, compared to conventional halogen and phosphorus-based flame retardants [133], its 2D structure provides only modest protection against fire in flammable materials. Functionalizing MXene with additional flame-retardant elements/groups/compounds can improve the flame-retardant efficiency of MXene. It is already impressive fire resistance. Numerous studies show how MXene reinforcement in polymers increases the flame-retardant efficiency of the base materials. For example, Jiang et al. developed a polyimide/MXene composite aerogel (PI@MXene) that demonstrated outstanding flame retardancy with self-extinguishing characteristic after 60 s of exposure to a flame. They had a 78% reduction in peak heat release rate (PHRR) [134]. Zhao et al. created a multifunctional polyimide/MXene/Ag_2Se nanowires (PMA) composite that exhibits outstanding flame retardancy with a limiting oxygen index (LOI) of 53% and PHRR lowered by more than 65% with a trigger time of 4–8 s when subjected to fire [135]. Ma et al. developed a fire-resistant wallpaper (FAW)

using MXene and lignocellulose nanofibrils (LCNF), achieving a 0.32 s alarm response and a consistent alarm signal up to 3073 s [136].

However, the majority of the known thermosensitive sensors works when subjected to fire or extreme temperatures (>150° C), showing that a warning response cannot be provided in time during the precombustion phase [137]. Furthermore, the preliminary programming required for a change in response temperature is often time-consuming and complicated, limiting its applicability in scenarios when variable response temperatures are needed [138]. So, a simple, self-cutting fire alerting device that can react to temperature changes is necessary. SMPs have distinctive characteristics, including the capability to adjust their T_g and a comparatively more straightforward program compared to SMAs. Due to these attributes, few research efforts have been made to advance fire-alerting devices based on SMPs. For example, in recent work, Zhang et al. developed a flame-retardant paper based on SMPU and MXene (SMPU/MXene) that demonstrated outstanding fire retardancy, quick self-extinguishing performance, and reductions of 49.8% and 66.0% in total heat rate (THR), and PHRR respectively [138]. The SMPU/MXene paper did not suffer from melt-dripping and was able to keep its original shape, in contrast to the neat SMPU paper (**Figure 8A**). Jaiswal et al. successfully created a unique heat detector/fire alarm system using a PU composite that functions as both an actuator and a heat sensor [101]. When tested under simulated under hot water and hot air conditions, the device performed effectively. The shape-switching property of pristine PU and PU composites, namely PU-Ti_2AlC+Ti_3AlC_2 MAX phase (PU-MAX_1), PU-Ti_3AlC_2 MAX phase (PU-MAX_2), and PU-Ti_3C_2 MXene (PU-MXene), was extensively investigated by the shape recovery phenomena in hot water and hot air environments. **Figure 8B** depicts the shape recovery of pristine PU and PU composites containing 0.25 wt% MAX_1, MAX_2, and MXene fillers in a hot water environment (70 °C) as a function of recovery time. During recovery, pictures were taken at angles of 30°, 60°, 90°, 120°, 150°, and 180°, demonstrating shape recovery with time. **Figure 8B** shows that pristine PU took approximately 42 s to fully recover from its deformed shape. However, the recovery time for PU

composites was significantly lowered, reaching as low as 17-18 s in PU composite samples. In hot air settings **(Figure 8C)**, the pristine PU took 170 s to fully recover from its deformed shape. On the other hand, the reinforcement of MAX and MXene phases improved PU's shape-switching ability, as demonstrated by a significant reduction in overall recovery time in PU-composites. The team also proposed a concept for a heat detector/fire alarm system based on the actuation capabilities of PU-composite. When tested under simulated heat and fire conditions, the device performed effectively. When the device is subjected to dry heat, the PU composite component senses heat and begins to swiftly return to its former shape, thereby shutting the circuit and activating the alarm, as evidenced by the LED light and sound buzzer turning on **(Figure 8D)**. The PU-MXene component of the proposed heat detector/alarm system can be reused several times, making the device simple and cost-effective while distinguishing it from commercially available devices. The device was also tested in a simulated fire environment in the laboratory where the device responded successfully when exposed to fire **(Figure 8E)**. Further, to carry out effective and secure thermal management, Gao et al. developed a flame-retardant composite phase change material (CPCM) composed of MXene, olefin block copolymer (OBC), and paraffin (PA) [83]. To enable quick heat transfer and dissipation, MXene increased CPCM's thermal conductivity to levels over 2.3 times that of PA. The flame retardancy of the samples was verified through a candle self-extinguishing experiment. **Figure 8F** demonstrates that highly flammable PA continues to burn without self-extinguishing. In contrast, S0 (0 wt% MXene) melts and collapses under high-temperature combustion because the network structure of non-flammable OBC cannot prevent the volatilization and release of PA. The escaped PA vapor is ignited by the wick and burns until all PA is completely consumed. However, samples namely S1 (5 wt% MXene), S2 (12.5 wt% MXene), and S3 (20 wt% MXene), self-extinguish entirely within 12 s while maintaining their morphological integrity. As the MXene concentration increases, the wick's flame becomes fainter. In this case, MXene acted as a physical barrier, containing the PA and effectively resisting high-temperature thermal evaporation. In a recent study, Yang et al. recently synthesized

biobased photothermal-responsive shape memory Polythioether/MXene (BEP-T-xM) nanocomposites with self-extinguishing properties [139]. These composites were created via in-situ thiol-ene photopolymerization of photopolymerizable MXene nanomonomer (MPS-MXene), bis(4-allyl-2-methoxyphenyl) phenyl phosphonate (BEP), and tris[2-(3-mercaptopropionyloxy)ethyl]isocyanurate (TEMPIC). The resulting polythioether/MXene composites exhibited excellent flame-retardant characteristics due to phosphorus-containing groups that form phosphate compounds during combustion. These compounds promote the dehydration of the matrix, creating a carbon protective layer that isolates oxygen and heat. The phosphorus groups also decompose into PO·, PO_2·, and HPO· free radicals, which capture combustion-sustaining hydroxyl and hydrogen radicals, disrupting the combustion chain reaction. Additionally, the nitrogen element in the thiol monomer TEMPIC releases inert gases like N_2 and NH_3 during combustion, diluting combustible gases and encouraging the formation of intumescent char residues.

Figure 8. (A) Flame procedure of **(a)** SMPU and **(b)** SMPU/MXene paper [138]. Shape recovery (recovery angle) of pristine PU, PU-MAX_1, PU-MAX_2, and PU-MXene composites as a function of time in **(B)** hot water, and **(C)** hot air. Heat detector/fire alarm device containing PU composite as an active component and its working mechanism in simulated **(D)** heat and **(E)** fire environments [101]. **(F)** Self-extinguishing experiment of PA and samples [83].

6.2. Actuation

SMPs offer a significant deal of potential for use in wearable technology and soft robotic systems due to their flexibility and light weight [140] [141]. SMPs offer a unique opportunity to construct untethered soft robots with programmable morphology and/or properties, reproducible actuation, and

enhanced multi-functionality. In addition, these materials open up new possibilities for deployable structures, such as deployable antennas, temporary architectures, spacecraft, and solar sails [142] [143] due to their high deformation and actuation capabilities [144] [145] [146]. For example, Song et al. fabricated an SMP blend system using TPU and polylactic acid (PLA) [147]. It was found that R_r and T_{trans} increase with increasing the concentration of PLA and TPU and programming temperature. There was no effect on the R_f by the temperature of the programming. Although SMPs can change the state easily, they have poor mechanical properties such as low actuation force, stiffness, and strength[148]. Incorporation of nanoscale fillers into SMPs enhances their mechanical, electrical, and thermal properties, ultimately producing improved actuators using the resulting SMP composites [41]. The fabricated SMPCs with improved performance are actuated using various actuation methods, including electricity, thermal, magnetic field, or light. For instance, Liu et al. demonstrated the electroactuated shape memory behavior of a 50 wt% antimony-doped TiO_2 (ATO/TiO_2)/SMPU sheet customized to "Π"-shaped structure following three recovery cycles [149]. According to research by Qi et al., the EVA/PCL/CNT system with 5 wt% CNTs was able to totally regain its original shape in 24 s at 20 V [150]. Yi et al reported the photothermal shape recovery actuation behavior in a bending and extension mode for the thin-walled carbon nanotubes (TWNT), RGO, and hyberbranched polyurethane (HBPU) composite [151]. The group asserted that the TWNT/RGO composition ratio and the amount of nanocarbon had a significant effect on the shape recovery behaviors of composites. Wang et al. fabricated thermally and electrically actuated crosslinked polycyclooctene (PCO), Multiwalled CNT (MWCNT), and Polyethylene (PE) [PCO-MWCNT/PE] nanocomposites. The developed nanocomposites show remarkable triple SME cycle via both heating and electrical command [152].

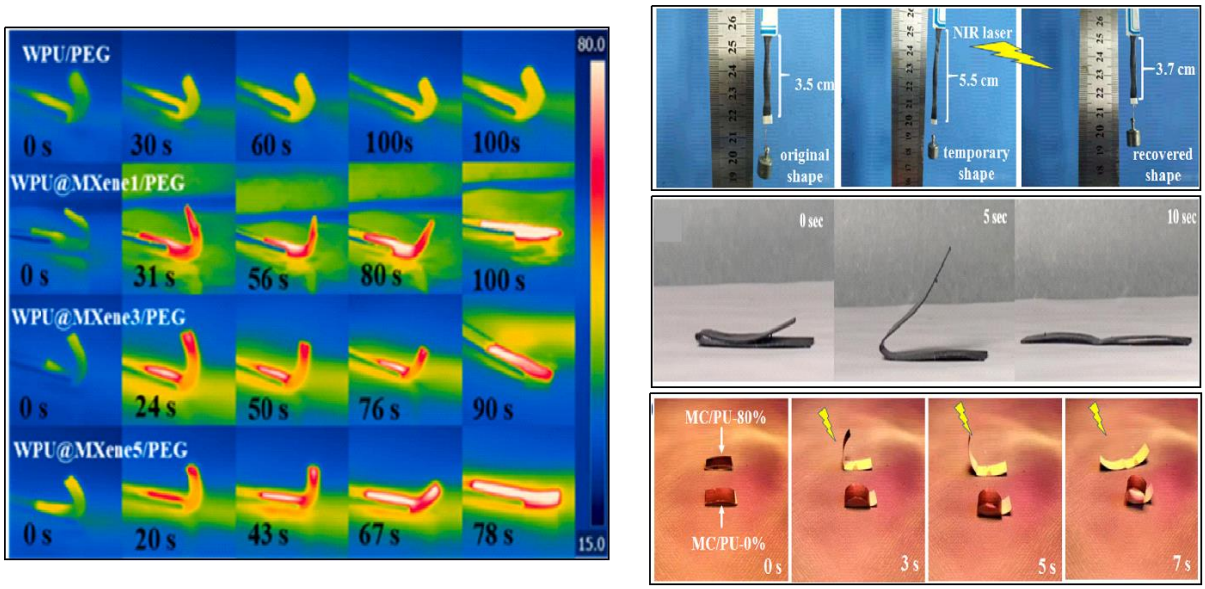

Figure 9. (A) Shape memory performance of 0 wt % and 2 wt % MXene composite [41]. NIR actuated shape recovery process in **(B)** extended, and **(C)** bent mode of MC/PU-80% shape memory composite [153]. **(D)** Light-actuated R_f and R_r perfomance of WPU/PEG and WPU@MXene/PEG [128].

MXenes were also incorporated into SMP matrix to increase their actuation properties. For instance, McLellan et al. fabricated TPU/PLA shape memory blend system with embedded Ti_3C_2 flakes [41]. The mechanical, thermal, and morphological properties of 3D/4D printed structures are greatly enhanced by the addition of Ti_3C_2 flakes (0.5 wt%). The composite exhibits excellent SME results at higher loadings (2 wt.%) of Ti_3C_2 flakes, quickly recovering 98% of its original position in less than 14 s **(Figure 9A)**. Wu et al. designed a new electrospun SMPU based actuator by coating MXene/cellulose nanocrystals (CNCs) (MC) composites onto fibril mats [153]. The actuator could raise a 265 times heavier object by 80% of its height in 10 seconds by optimizing composite formulas. **Figure 9B** and **9C** show the actuation of the MC/PU-80% in the extended and bent states under NIR light. While the control sample stayed bent, MC/PU-80% was able to finish recovery in almost 7 s. According to Hu et al., the WPU@MXene/PEG-PCM composite is easily bendable at temperatures above the melting point of PEG of 70 °C [128]. The transient "U" shape can be effectively secured once it has cooled to room temperature (25 °C) and has been relieved of external stress. Surprisingly, WPU/PEG maintains its transient "U" shape when the NIR light is turned on, but all

WPU@MXene/PEG-PCM composites completely recover to their original straight shape **(Figure 9D**). Also, Meng et al. synthesized double-network hydrogel Ag/$Ti_3C_2T_x$@gelatin/poly(dimethyl acrylamide) (PAAm) that can also be used to design soft actuators [154]. These investigations have a significant influence on the discovery of intelligent polymers as soft actuators or robots for remote delivery. Li et al. developed a high-performance MXene@CS@TPU composite-based sensor with compressive strains of up to 85% at 245.7 kPa, a 19-ms response time, repeatability for 5000 compression-release cycles, and a low detection limit (LOD) of 30 N at 9 Pa [71]. Yang et al. fabricated a multifunctional MXene/polyurethane mat-based stable strain sensor demonstrating high sensitivity, tuneable sensing range, and low LOD [155]. The sensor can sense a variety of stimuli in addition to lateral strain, including normal pressure, bending, and even minor vibrations. **Figure 10A** shows the sensor's responses when stretched to various strains from 20% to 100% (the inset shows strains from 0.1% to 10%). Additionally, Xie et al. created a long-lasting shape memory fiber strain sensor for measuring human mobility utilizing composites made of MXene, CNTs, and EVA **(Figure 10B)** [85]. This sensor offers excellent sensitivity, rapid response times, and a wide strain measurement range. In case of damage, it can be restored to 92% mechanical and 94% electrical performance through a 2 min heating or 5.4 s infrared light treatment. Pu et al. created multilayered ultrasensitive AgNW/WPU-MXene fiber strain sensors with a broad working range [156]. **Figure 10C** illustrates relative resistance changes from 0% to 60% strain, with an inset highlighting the curve within the 0–20% strain range.

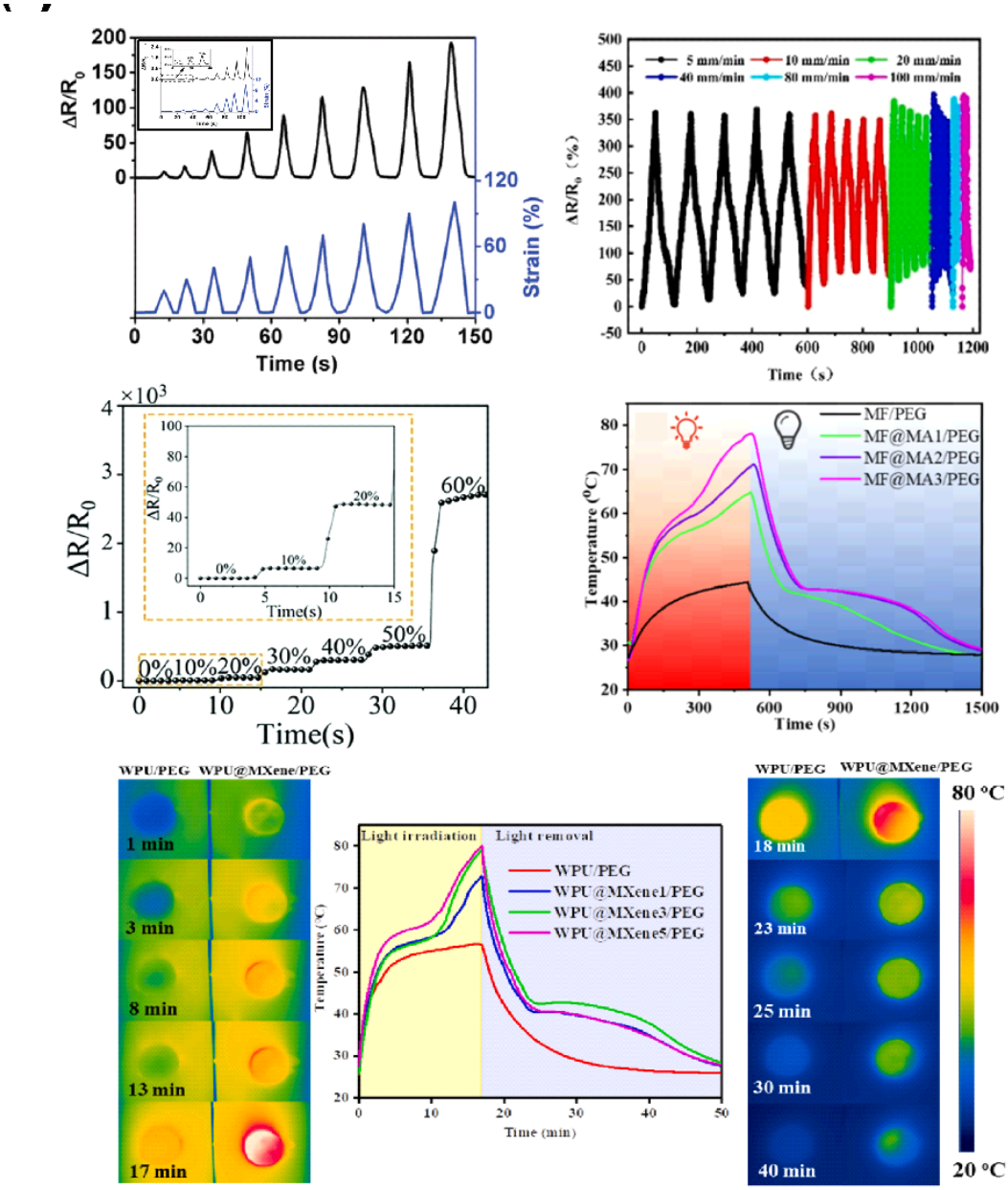

Figure 10. (A) Responses of the MXene/PU-based mat sensor upon stretching to different strains varying from 20%–100% (inset showing strains ranging from 0.1% to 10%) [155]. **(B)** Change in MXene/CNTs/EVA fiber relative resistance at a tensile strain of 30% under various tensile speeds [85]. **(C)** Change in relative resistance at different strains from 0% to 60% (inset: 0–20% strain curve) [156]. **(D)** The energy storage and release performances of MF@MA/ PEG [157]. **(E)** WPU/PEG and WPU@MXene/PEG performances in energy storage and release. The change in temperature during heating and cooling operations were captured in infrared photos and the associated temperature-time curves [158].

6.3. Energy Storage

The identification of PCMs as potential latent heat storage materials has generated a great deal of demand in the areas of energy-efficient structures, thermal control of electronic devices, and healthcare

settings [159, 160]. However, PCMs have some significant disadvantages in real-world applications, such as easy leakage above the PCMs' melting point [161], low TC which slows the heat storage speed [162, 163], a lack of light and electric responsiveness [164], and high rigidity [165], which prevents PCMs from being installed in confined spaces or coming into close contact with objects. In this approach, a number of researchers have looked into carbon-based materials to create shape-stable PCMs with photothermal conversion and energy storage characteristics [166] [167] [168].

MXene has received much research attention compared to carbon-based materials because of its extraordinary photo absorption capacity, resulting in improved solar-to-thermal conversion performance of PCM composites [169]. For instance, Fan et al. developed a new PEG /$Ti_3C_2T_x$ layered PCM composite with excellent photothermal storage performance, high energy storage density, and shape stability before and after phase transformation [170]. Lu et al. fabricated a PEG @MXene composite that exhibited remarkable photothermal and electrothermal conversion with thermal energy storage properties [171]. Lin et al. infused PEG with a lightweight MXene aerogel, resulting in PCM composites with efficient solar energy to heat conversion [172]. Mo et al. developed a unique polyethylene glycol (PEG 2000) PCM composite anchored in a $Ti_3C_2T_x$@PVA foam scaffold, which exhibits good photothermal conversion efficiency, high thermal conductivity, thermal energy storage ability, and structural stability [173]. However, due to the brittleness of MXene scaffolds, these MXene-based PCMs could have high stiffness and limited flexibility. Moreover, due to the rigidity of PCM composites, the installation would be problematic, and contact with target device surfaces would be insufficient, significantly limiting applications in thermotherapeutic devices and flexible wearable heaters [157]. Therefore, the selection of flexible MXene scaffolds is crucial for the development of PCM shape memory composites. One successful way to fabricate MXene aerogels with high porosity and exceptional elasticity is to combine MXene with water-soluble polymers. For instance, Shao et al. developed a novel PCM composite by incorporating MXene-coated melamine foam (MF@MXene) into PEG, which exhibited excellent shape fixation and recovery effects, with excellent encapsulation

properties, and effective solar energy to thermal conversion [157]. Furthermore, He and colleagues recently reported the preparation of multifunctional PCM composites by vacuum-impregnating porous MXene/silver nanowires (MA) hybrid sponges with PEG [125]. Being an excellent photon absorber, the MA hybrid fillers provided the MF@MA/ PEG composites the ability to convert and store light into thermal energy (**Figure 10D**). The composite also exhibited considerable photoinduced shape memory function and had high R_f (~100%) and R_r (~100%) values. Hu et al. developed a photoinduced and flexible PCM composite by encapsulating PEG in a polyurethane (WPU)/MXene aerogel [158]. The composite PCM was characterized by excellent dimensional stability, impressive phase change enthalpy value, outstanding solar to thermal energy conversion performance (**Figure 10E**), and energy storage potential. The composite's R_r value and self-healing efficiency were also determined to be 100% and 82.9%, respectively.

6.4. Electromagnetic Interference (EMI) Shielding

The exponential expansion of technology and electronic devices has led to EMI caused by various sources such as radio frequency interference, electromagnetic (EM) coupling, electrostatic discharge, and leakage/induction [174]. High-energy EM signals have increased due to the adoption of 5G technology, which causes mutual interference that impairs device performance [175]. EMI adversely affects electronic devices and electrical systems, impacting communications, military, medical, and remote sensing industries [176]. Prolonged exposure to EM radiation poses health risks like cancer, asthma, heart disease, migraines, and miscarriages [177]. Effective reduction of electromagnetic radiation is needed to address this risk. Until now, metals and composites have been used as EMI shielding materials, that are highly effective due to their conductivity, mechanical properties, and permeability. However, these materials also had disadvantages such as low flexibility, high density, and susceptibility to corrosion. In recent years, researchers have explored polymeric materials because of their flexible, lightweight, processable, chemically resistant, and scalable properties beyond metallic materials' limitations. When appropriate conductive fillers, including carbon-based

nano/microstructures, are added, intrinsically conductive polymer-based materials provide better corrosion resistance and electrical conductivity [178]. These fillers create an electrically conductive network in a polymer matrix, which enables light EMI shielding. For better EMI shielding, achieving a percolation threshold at low filler content is essential. Surface modification, surfactants, and functionalization can all help to create an appropriate filler dispersion. Structural design and hybrid filler composites also contribute to excellent shielding efficiency. MXenes have been identified as viable candidates for EMI shielding due to some exceptional characteristics, such as high electrical and thermal conductivity, layered structure, flexibility, and mechanical stability. On the other hand, shape memory allows SMPs to adapt to different EMI shielding requirements, making them adaptable and versatile. However, oinadequate electrical properties of SMPs' restrict their utility in EMI shielding applications. Fortunately, the discovery of MXenes with superior inherent metallic conductivity, which does not require difficult chemical reduction, opens the possibility of using them as substitutes for other EMI shielding materials [179]. Shahzad et al. were the first to report the electrical conductivity of $Ti_3C_2T_x$-based films, which is 4600 S/cm for pure $Ti_3C_2T_x$ films, as well as their outstanding EMI SE and high SSE/t of 30830 dB cm^2 g^{-1} [180]. The ability of MXene film to shield EMI was effective up to 92 dB.

MXenes are capable of interacting with polymer chains due to the numerous active functional groups that are present on their surface. This allows for the fabrication of high-geared EMI-shielding polymer composites [181] [182] that are flexible but structurally robust. According to recent reports, Liu et al. developed a shape-stabilized MXene/ PCM composite with an improved thermal conductivity of 0.74 W/mK and a great EMI SE of 64.7 dB in the X-band [183]. However, these MXene composites are less flexible and non-healable and require constant force to maintain compression, further reducing EM shielding, which is unfavorable for their use in modern electronics. As a result, including shape memory functionality into shielding composites offers a simple method to modify the shielding effectiveness by altering the shape triggered by an external stimulus. For instance, Yuan et al. prepared

single-sided and double-sided MXene/PU fabric (SMPUF/DMPUF) that demonstrated good mechanical properties and EMI SE of >~20 dB at a stretching process within 30% deformation in the X band, which makes it a potential candidate in wireless sysytems, robotics, and flexible electronic devices [184]. The shielding process of the SMPUF and DMPUF is shown in **Figure 11A**. A TPI-M/CF composite with outstanding thermally and electrically driven shape memory capabilities was developed by Jia et al. It can be easily distorted and restored when heated over the melting temperature and fixed to a transient shape at low temperature [185]. The composite showed increased EMI SE of ~25.3-44.7 dB with intelligent function-tunable or function-switchable characteristics. In another study, Jia et al. constructed an MXene-based conductive polymer composite (CPC) foam with outstanding EMI SE of ~23.5-39.8 dB [186]. Moreover, under 0-40% compressive strain, the SE value of the composite foams can fluctuate between ~27.7 and ~16.2 dB **(Figure 11B),** indicating a significant usage in EMI shielding. Additionally, the composite foams can survive several compressions and can flex between 20 and 60% before returning to their original thickness. Further, Lu et al. fabricated a self-healing castor oil-based WPU/MXene coating with remarkable EMI SE (51 dB) and outstanding shape memory capability **(Figure 11C)** [129]. At such a low elongation break (30%), the mechanical property rises to 15 MPa while still possessing the shape memory and self-healing ability. In a recent study, He et al. prepared multifunctional MF@MA/PEG composites that demonstrated good thermal and electrical conductivity, high dimension retention ratio, and better latent heat **(Figure 11D)** [125]. The composite exhibited high R_f and R_r values, with significant photoinduced shape memory function. The composites may provide tunable EMI SE from 12.4 to 30.5 dB by including shape memory properties. Liu et al. fabricated nanocomposite films incorporating polyurethane and MXene, featuring a structure reminiscent of nacre, designed for EMI shielding. In instances where the polyurethane content reaches 20 wt.% and the tensile strength measures approximately 100 MPa, the SE of this film reaches an impressive 49.4 dB [58].

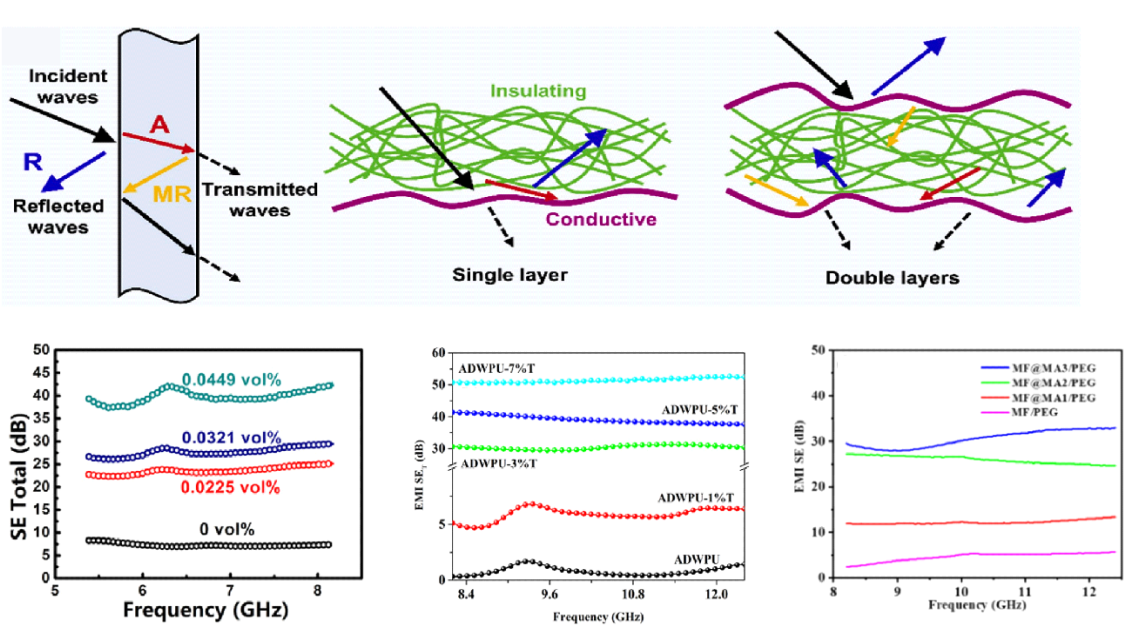

Figure 11. (A) EMI shielding mechanism of the SMPUF and DMPUF fabric [184]. **(B)** SE total of PDMS-PANI/mPP foam with different MXene content [186]. **(C)** SE total of the films on the X-band with various MXene content [129]. **(D)** SE total of MF/PEG and MF@MA/PEG [125].

6.5. Biomedical Applications

SMPs are increasingly being explored in the domain of biomedical due to their advantageous qualities, which include low density and weight, outstanding flexibility, and biocompatibility [187]. By changing the porosity, orientation, and microstructures, SMPs can be tailored to mimic biological materials such as natural extracellular matrices [188]. SMPs find applications in a variety of biomedical processes, including drug delivery [189] [190], tissue engineering [191] [192], wound dressing [193], fabrication of biomedical devices, and medical imaging [194]. However, it's worth noting that the operational principle of SMPs primarily involves exposure to heat, causing the polymer to undergo creep under stress due to the limited lifespan of chain linkages within the polymer structure at elevated temperatures [188]. In addition, SMPs have low mechanical strength and poor surface wettability. Therefore, fillers are often added to improve these properties [187].

MXenes possess some attractive properties, like hydrophilicity, antimicrobial nature, biocompatibility, and non-toxicity to living organisms [195], which makes them perfect for biomedical applications [196]. Also, MXenes are known for their robust absorption characteristics in the near-infrared (NIR)

spectrum. This attribute unlocks exciting promises for applications in both in vivo photoacoustic imaging (PAI) and photothermal therapy (PTT), particularly within the first or second biological window. [197]. MXenes are extensively researched and developed for a variety of biological applications because of their fascinating physicochemical characteristics, including drug delivery systems [198] [199] [200], bioimaging [201], therapeutic diagnostics [202] [203], implants [204] [205], tissue engineering [206] [207] [208], and antibacterial agents [209].

6.5.1. Drug Delivery

SMPs play an important role in drug delivery. Lendlein et al., for instance, used SMPs in a drug delivery system to provide regulated drug release [210]. Initially, the SMP completely envelops the drugs on its surface, providing complete coverage. Once the drug delivery system enters the body, the SMP gradually releases a specific dose of the drug at a controlled rate by precisely controlling the rate of reforming. This intelligent control enables targeted drug release at predetermined sites. In addition, Ameer et al. developed a novel sequence of biodegradable elastomers derived from citric acid. These innovative elastomers also exhibit a SME, enabling their use in drug-release systems that activate at therapeutically appropriate temperatures [211]. The temperature-dependent delayed release was observed when tiny hydrophobic aliphatic diols were added to these elastomers. Moreover, Li et al. developed a drug-releasing SMP relying on poly(methyl methacrylate-co-butyl acrylate). The SMP properties of this polymer can be activated by ultrasound stimulation while concurrently releasing a model compound of copper sulfate, which is present at a concentration of 5 wt% [212]. Surprisingly, drug delivery can thus be stopped at any time, with partial shape recovery. Another application for SMPs as drug delivery systems can be seen in cardiovascular stents. Wache et al. were the first to propose drug-eluting stents made from SMPs. The injection-molded prototype stent was made of TMPU [213]. Later, Gall and Yakacki et al. began to use thermosetting (meth)acrylates to fabricate SMP stents [214]. Sun et al. also made a PLA-based biodegradable coil stent that once warmed to body temperature, the spiral stent returned to its original shape [215]. In addition, Chen et al. made a

biodegradable stent possessing shape memory properties using a blend of chitosan films combined with glycerol and poly(ethylene oxide), all cojoined with an epoxy resin [216]. When hydrated, this stent can rapidly expand, transitioning from its crimped (temporary) state to a fully expanded (permanent) state in just 150 s. Yang et al. have made biodegradable crosslinked networks using PEG and PCL copolymers which are biocompatible. These networks exhibit good shape memory properties with T_m close to body temperature, making them highly suitable for biomedical applications [217]. A six-arm PEG-PCL polymer network was employed by Gong et al. to build a bi-directionally recoverable SMP that might be used as a reversibly converted micrometer-sized drug delivery carrier [218].

MXenes, with their high surface area and tunable surface chemistry enable efficient loading and release of therapeutic agents, making them highly effective in drug delivery [219]. Their inherent electrical conductivity can be leveraged for stimuli-responsive drug delivery systems, where drugs are released in response to external signals such as light or magnetic fields. Moreover, the ability of MXenes to form stable colloidal suspensions enhances their dispersibility in biological environments [220], facilitating targeted drug delivery and minimizing off-target effects. These combined attributes position MXenes as a promising material for advanced drug delivery systems.

6.5.2. Tissue Engineering

In bone tissue engineering, SMPs offer minimally invasive implantation and good self-adaptation in bone defects [221]. For example, Zhai et al. have engineered composite scaffolds composed of poly(N-acryloyl glycin amide) and nanoclay [222]. These scaffolds have demonstrated the ability to stimulate osteogenic differentiation and facilitate the regeneration of bone tissue, showcasing their potential in regenerative medicine [223]. Melissa A. Grunlan et al. devised a SMP scaffold through photo-crosslinking PCL [224]. When the PCL material was heated to, or above, its T_g, the previously rigid cylindrical framework softened, allowing it to be mechanically shaped into irregular forms. Upon cooling, this altered shape was retained, illustrating the remarkable shape memory properties of the

material. Wang et al. printed 3D shape memory scaffolds with superparamagnetic iron nanoparticles to induce osteogenic induction [225]. In a recent article, Xuan et al. discussed the use of SMPs for cartilage regeneration. They used bioactive kartogenin in their polymer, which promotes cartilage regeneration [226].

MXene can play significant and advantageous roles in developing novel inorganic composite materials for bone tissue regeneration, particularly for enhancing mechanical properties, biocompatibility, and osteoinductivity [227]. Xie et al. have introduced a multifunctional implant Sp@MXGelMA that exhibits improved cytocompatibility, osteogenesis, and osseointegration [204]. Chen et al. investigated the impact of OTES-$Ti_3C_2T_z$/PLA on bone formation by combining $Ti_3C_2T_z$ MXene with PLA [228]. The prepared membrane was tested on mice and shown to simultaneously improve cell adhesion, proliferation, and osteogenic differentiation.

6.5.3. Wound Healing

Shape memory nanofibers have also found applications in wound treatment. Li et al. developed an electroactive PU-SMP for wound dressings [229]. In addition to its shape memory capabilities, which can help heal injured or open wounds without additional suturing, the material exhibited radical scavenging properties. Zhao et al. synthesized a hemostatic injectable antimicrobial conductive SMP [230]. The SME is used here to compensate for uneven wounds in combination with pressure after polymer expansion. MXene, an excellent photothermal agent, can effectively treat wound infections in photothermal therapy. Due to its 2D structure, MXene increases the effective contact between bacteria, thus improving antibacterial efficacy. Xu et al. fabricated a nanofiber membrane comprising of amoxicillin (AMX), MXene, and PVA [231]. The developed membrane showed high antibacterial activity and improved wound healing. As a photothermal component [232], MXene has attracted great interest because it exhibits internal light-to-heat conversion efficiency of nearly 100%, and can be used in wound dressings, as it has good light-transmitting effect that can repair skin repair [233] [234]. Hu et al. also demonstrated good photothermal characteristics of MXene based shape memory hydrogel

as a wound dressing that exhibited a surface temperature of 86.4 °C after 20 s of light exposure, making it ideal for skin repair treatments [121]. In a recent study, Wu et al. developed a hemostatic antibacterial chitosan/N-hydroxyethyl acrylamide (NHEMAA)/$Ti_3C_2T_x$ (CSNT) cryogel through physical interactions and spontaneous NHEMAA condensation [235]. Pure chitosan cryogel (CS) and chitosan/NHEMAA cryogel (CSN) were also prepared for comparison. The synergistic effect of hydrophilic, negatively-charged MXene and positively charged chitosan resulted in dense cross-linking networks in the CSNT cryogel. The CSNT cryogel exhibited a large pore structure (~99.07%) and superfast water/blood-triggered shape recovery, making it ideal for wound filling, which is ascribed to the hydrophilic groups of $Ti_3C_2T_x$ that enhnaced the pore structure and provided a capillary effect. The cryogel showed good photothermal antibacterial activity, biosafety, and effective in vivo wound healing. When tested against *Escherichia coli (E. coli)* and *Staphylococcus aureus (S. aureus)*, the CS, CSN, and CSNT cryogels demonstrated a progressive decrease in colony numbers, which can be attributed to their tiny structures and active sites on the pore surface. Following 100 s of NIR irradiation, the CSNT cryogel (NIR-CSNT) showed few colonies, indicating higher photothermal antibacterial efficacy, potential for wound infection prevention, and improved blood-clotting capabilities as hemostatic materials. A variety of elements contribute to the CSNT cryogel's quick hemostatic effect. The cryogel's complex porous structure absorbs plasma and traps hemocytes, creating a blood clotting barrier. Protonated amino groups interact with blood cells, causing platelets to activate and aggregate. The negatively charged $Ti_3C_2T_x$ stimulates platelet activation and the clotting cascade, while its lipid affinity increases lipid buildup in blood, all of which contribute to the cryogel's hemostatic properties. Furthermore, chitosan hindered MXene oxidation, guaranteeing the long-term preservation of the MXene-reinforced cryogel by adhering to the chitosan chain via electrostatic interaction and preventing MXene oxidation.

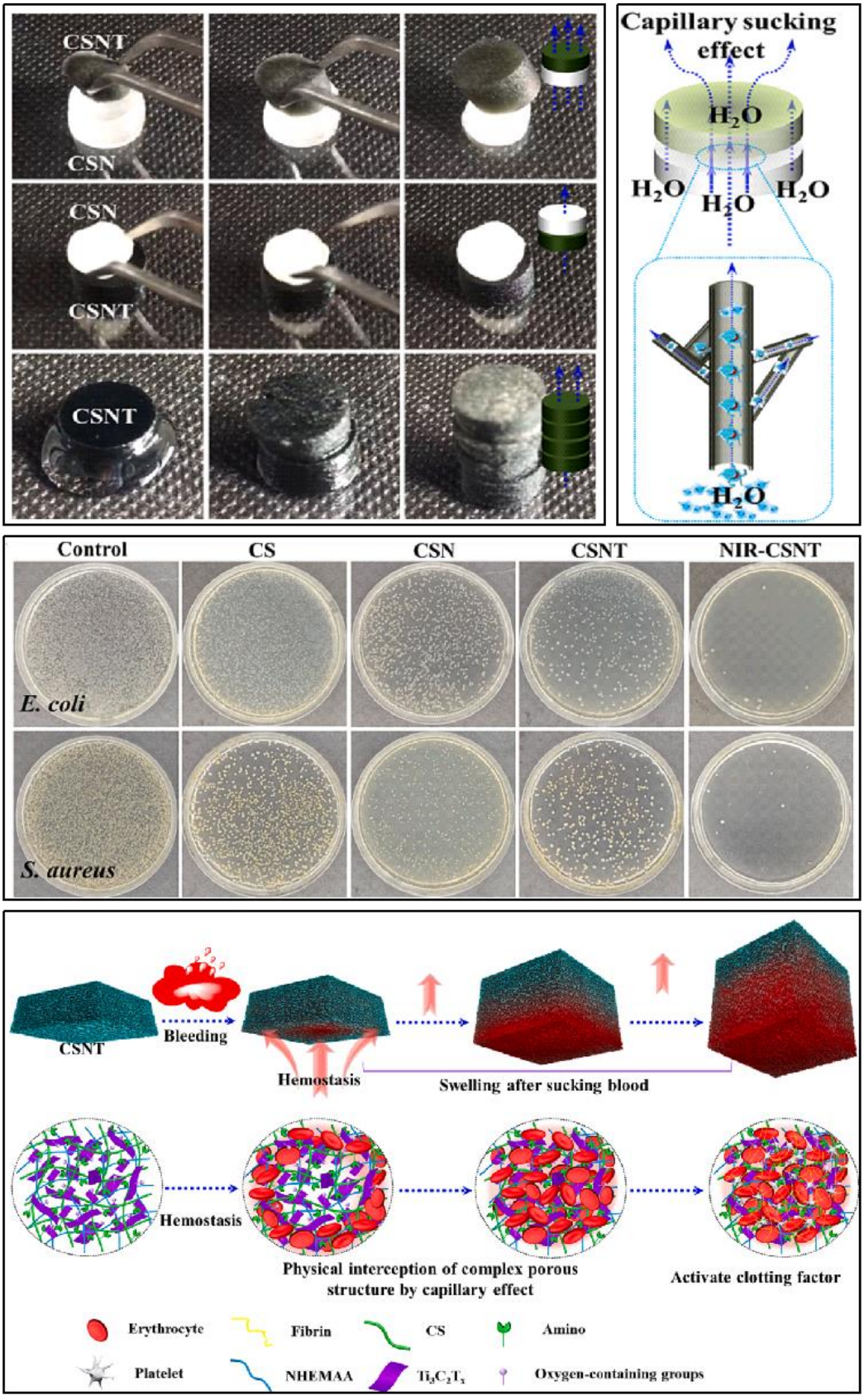

Figure 12. (A) Capillary sucking test of CS, CSN and CSNT cryogels. **(B)** Photothermal antibacterial activity of control, CS, CSN and CSNT cryogels. **(C)** Hemostatic mechanism of the CSNT cryogel [235].

6.5.4. Other Biomedical Applications

SMPs could also be used as cell/drug/protein transporters. Because of their injectability and shape memory properties, SMPs can be used in bioprinting, minimally invasive surgery, and precision medicine [236]. However, MXene-incorporated SMPs have hardly been explored in the abovementioned domains. The synergism among SMPs and MXenes can be greatly useful in bone tissue formation, wound healing, and drug delivery. Some researchers have focused on improving/modifying the properties of MXene materials to explore other biomedical applications. For example, the potential of Mo_2C-PVA nano-flocks for theranostics in nanomedicine was examined by Feng et al. They discovered that they exhibit fascinating broad absorption bands covering the NIR in both the I and II regions in addition to having great biocompatibility and quick degradability [237]. The great photothermal conversion increased the prospects of photothermal cancer ablation with MXene-based polymers. Wang et al. created a MXene-based shape-programmable supermolecular nanocompsite film by combining MXene and PVA [115]. MXene acts as crosslinking sites in the nanocomposite and provides additional intermolecular hydrogen bonding contact with PVA, which gives this film a strong shape-fixing property. In another report, Han et al. found that Ti_3C_2 MXene surface modification has an ablating temperature of 68.5 °C by NIR laser and a 74.6% inhibition rate, effectively killing the tumor cell as a result of the synergistic impact [238].

7. Perspective on MXene and other Carbon-based fillers

MXene has emerged as a viable filler for improving the characteristics of SMPs. These 2D transition metal carbides, nitrides, or carbo-nitrides have a distinct set of mechanical, electrical, and thermal characteristics that make them ideal for improving the performance of SMPs. MXenes have a large surface area, high electrical conductivity, and extraordinary high mechanical strength, which together lead to considerable improvements in the functioning and efficiency of SMPs. MXenes have a distinct set of surface functional groups like OH, -F, and -O on their surface that allows for the flexible chemical modifications, which enhance their compatibility with different polymer systems [239]. This

customizable surface chemistry may be used to increase adhesion and interfacial interaction between MXenes and the polymer matrix, resulting in superior mechanical and thermal performance. Furthermore, the chemical adaptability of MXenes, which may be adjusted by changing the transition metal and surface terminations, can provide a great degree of control over the composite material's ultimate qualities. On account of this, in addition to the most often used Ti_3C_2 MXene, additional MXenes such as vanadium carbide (V_4C_3), niobium carbide (Nb_2C), and molybdenum carbide (Mo_2C), among others, provide a wide range of functionalities that may be adapted for specific applications. For instance, incorporating V_4C_3 MXene into SMP matrix, can significantly enhance electroactive properties due to its excellent conductivity and high surface area, making the composite more suitable for applications like sensors, actuators, and energy storage devices [240] [241]. Nb_2C MXene, with its outstanding mechanical strength and stability, can potentially increase the longevity and mechanical characteristics of polymer matrix [242], making it a great contender for several applications, including batteries, supercapacitors, photocatalysts, and photovoltaics. In comparison to Ti_3C_2 MXene, Nb_2C MXene show higher electroconductivity and wettability due to its lower Fermi energy level [244]. Mo_2C MXene, known for its strong catalytic capabilities, can improve the thermal and chemical durability of polymers [245] [246]. Overall, the choice of MXene is determined by the desired improvement in the polymer matrix, with each MXene contributing specifically to the polymer's characteristics, which include mechanical strength, electrical conductivity, thermal stability, and catalytic activity. In contrast, carbon-based fillers, such as graphene and CNTs, which have remarkable mechanical, thermal, and electrical characteristics, are less capable of surface functionalization [243]. Graphene and CNTs have inert sp^2-hybridized carbon structure [244], with few reactive sites for functionalization [245]. This stability, while is useful for retaining their fundamental features, poses a challenge for introducing functional groups. Also, MXene and graphene fillers exhibit distinct hydrophilicity behaviors that significantly influence the properties of SMPCs. MXene is known for its high hydrophilicity due to the presence of polar functional groups (-OH, -F, and -O) which enhances

its dispersion in polar solvents and its interaction with hydrophilic polymer matrices [246] [247], leading to improved mechanical properties and better stress transfer within the composite [248] [249] [250]. Moreover, efforts are also been made to disperse the hydrophilic MXene into hydrophobic polymers as well. In this respect, Liu et al. reported the uniform dispersion of hydrophilic $Ti_3C_2T_x$ MXene into hydrophobic polybenzoxazine (PBZ) [246]. The team enhanced the amount of the -F, and -O terminations on the surface of $Ti_3C_2T_x$ MXene by different etching conditions, and prepared the composite by solvent-assisted drop-casting and annealing method. The formation of H-bonds between MXene and BZ accelerated the ring-opening polymerization and enhanced the interfacial interactions. The composites exhibited enhancement in tensile strength of 22.1%, impact strength of 50%, and thermal conductivity of 67.3% when the filler content was only 2 wt%. In contrast, graphene, although it can be modified to exhibit hydrophilic properties, is intrinsically hydrophobic. This intrinsic hydrophobicity can lead to challenges in dispersion within hydrophilic polymers [251], often requiring functionalization to improve compatibility and dispersion. Further, MXenes' superior conductivity allows for efficient thermal and electrical routes inside the polymer matrix, resulting in rapid and more uniform heating and activation of the shape memory response. Gogotsi and team created MXene films that are flexible, foldable, electrically conductive, hydrophilic, and very stable in water [252]. Among other findings, y discovered that pure MXene sheets conduct electricity better and hold more charge than graphene and carbon nanotube "paper." $Ti_3C_2T_x$ films have electrical conductivities of 2.4×10^5 S/m, which is significantly greater than graphene or CNT "paper" [252]. This feature is very useful in SMPs, where electrical conductivity may be used for electroactive SMEs.

8. Challenges and Future Prospects

MXene-enhanced SMPCs are a promising way to advance materials science, with applications ranging from flexible electronics to biomedical devices and smart fabrics. MXenes' outstanding electrical conductivity, mechanical strength, and adjustable chemistry, along with polymer shape memory capabilities, provide a diverse foundation for novel technologies. Despite their great promise, a number

of scientific barriers must be overcome before these materials may be applied in the real world. First of all, the costly manufacturing of MXene is a significant limitation, as it hinders widespread adoption and scalability for commercial applications. A promising solution is the development of cost-effective fabrication techniques with simpler etching processes using sustainable synthesis approaches. These advancements can lower manufacturing costs, improve scalability, and make MXene more accessible for a wider range of applications, allowing it to reach its full potential in a variety of sectors. Another most significant issues are the intrinsic instability of MXenes, namely their vulnerability to oxidation due to their hydrophilic character. This deterioration can considerably reduce the performance and lifetime of MXene-enhanced composites, making it critical to develop stabilization approaches for these materials. Surface functionalization approaches, such as coating MXenes with protective layers or incorporating stabilizing agents, should be introduced for increasing the oxidation resistance and polymer matrix compatibility. For instance, Ji et al. conducted a study where they functionalized Ti_3C_2 MXene with silylation reagents, specifically (3-aminopropyl)triethoxysilane (APTES), to modify its hydrophilicity [253]. By functionalizing Ti_3C_2 with APTES, the APTES molecules attach to the surface of Ti_3C_2 through their silane groups, forming a protective layer that prevents water molecules from coming into direct contact with the MXene surface, making it less prone to degradation in aqueous environments. Similarly, optimizing the dispersion of MXenes within the polymer matrix is another essential issue to be addressed. MXenes agglomerate due to their high surface energy, resulting in heterogeneous composite structures that can degrade mechanical and functional qualities. Techniques such as chemical doping, interfacial engineering, and refinement of fabrication methods like solution mixing, in situ polymerization, etc can improve interfacial bonding and enhance the overall properties of the composites. Researchers have examined a variety of functionalization techniques, including the use of PEDOT [254], PVA [255], amino silanes [256], and dopamine [257] [258]. For instance, Liu et al. synthesized ultra-high specific surface area aerogels with nitrogen-enriched $Ti_3C_2T_x$ nanosheets for high-performance supercapacitor electrodes [259]. The researchers described a simple technique that

combines nitrogen doping with 3D structure creation on MXenes to avoid MXene nanosheet restacking while also improving electrochemical performance by enhancing the number of active sites, and electron mobility.

To overcome all the aforementioned bottlenecks, multidisciplinary research initiatives are critical. Collaboration among materials scientists, chemists, and engineers can lead to the creation of innovative MXene-enhanced composites with tailored characteristics for particular applications. Furthermore, establishing scalable and cost-effective manufacturing procedures is critical for large-scale production and commercialization of MXene-SMP composites. In conclusion, while MXene-enhanced SMPCs hold immense potential for revolutionizing various industries, overcoming the existing scientific and technical obstacles is critical to their successful commercialization. By focusing on stability, compatibility, interfacial bonding, and environmental sustainability, researchers can unlock the full potential of these advanced materials.

Declaration of Competing Interest

The authors declare no conflict of interest.

Data Availability

The data that support the findings of this study are available at reasonable request from the corresponding author.

Acknowledgments

The authors thank the Director Council of Scientific and Industrial Research (CSIR)-Advanced Materials and Processes Research Institute (AMPRI), India, for his kind support. This research was supported by the Council of Scientific and Industrial Research (CSIR), India, through the MLP 303 project. S. J. acknowledges CSIR, India, for providing financial support through the JRF/SRF fellowship.

References

[1] D. Rokaya, H.E. Skallevold, V. Srimaneepong, A. Marya, P.K. Shah, Z. Khurshid, M.S. Zafar, J.J.J.o.C.S. Sapkota, Shape Memory Polymeric Materials for Biomedical Applications: An Update, 7(1) (2023) 24.
[2] M. Behl, A.J.M.t. Lendlein, Shape-memory polymers, 10(4) (2007) 20-28.
[3] F. Pilate, A. Toncheva, P. Dubois, J.-M.J.E.P.J. Raquez, Shape-memory polymers for multiple applications in the materials world, 80 (2016) 268-294.
[4] M. Lei, Z. Chen, H. Lu, K.J.N.r. Yu, Recent progress in shape memory polymer composites: methods, properties, applications and prospects, 8(1) (2019) 327-351.
[5] T. Mu, L. Liu, X. Lan, Y. Liu, J.J.C.S. Leng, Technology, Shape memory polymers for composites, 160 (2018) 169-198.
[6] W. Wang, D. Liu, Y. Liu, J. Leng, D.J.C.S. Bhattacharyya, Technology, Electrical actuation properties of reduced graphene oxide paper/epoxy-based shape memory composites, 106 (2015) 20-24.
[7] H. Lu, Y. Yao, W.M. Huang, D.J.C.P.B.E. Hui, Noncovalently functionalized carbon fiber by grafted self-assembled graphene oxide and the synergistic effect on polymeric shape memory nanocomposites, 67 (2014) 290-295.
[8] J. Vishwakarma, S. Jaiswal, P. Bharti, C. Dhand, R. Kumar, S.A.R. Hashmi, A.K. Srivastava, N. Dwivedi, Competing and decisive roles of 1D/2D/3D sp2-carbons in controlling the shape switching, contact sliding, and functional properties of polymers, Materials Today Chemistry 25 (2022) 100960. https://doi.org/https://doi.org/10.1016/j.mtchem.2022.100960.
[9] P. Kumar, C. Dhand, N. Dwivedi, S. Singh, R. Khan, S. Verma, A. Singh, M.K. Gupta, S. Kumar, R. Kumar, A.K. Srivastava, Graphene quantum dots: A contemporary perspective on scope, opportunities, and sustainability, Renewable and Sustainable Energy Reviews 157 (2022) 111993. https://doi.org/https://doi.org/10.1016/j.rser.2021.111993.
[10] X. Qi, W. Wang, H. Dai, Y. Zhu, Y. Dong, S.-Y. Fu, Q. Ni, Y. Fu, Multifunctional two-way shape memory RGO/ethylene-vinyl acetate composite yarns for electro-driven actuators and high sensitivity strain sensors, Composites Part A: Applied Science and Manufacturing 169 (2023) 107521. https://doi.org/https://doi.org/10.1016/j.compositesa.2023.107521.
[11] Z. Li, X. Qi, L. Xu, H. Lu, W. Wang, X. Jin, Z.I. Md, Y. Zhu, Y. Fu, Q. Ni, Y. Dong, Self-Repairing, Large Linear Working Range Shape Memory Carbon Nanotubes/Ethylene Vinyl Acetate Fiber Strain Sensor for Human Movement Monitoring, ACS Applied Materials & Interfaces 12(37) (2020) 42179-42192. https://doi.org/10.1021/acsami.0c12425.
[12] Y.-M. Ha, Y.-O. Kim, Y.-N. Kim, J. Kim, J.-S. Lee, J.W. Cho, M. Endo, H. Muramatsu, Y.A. Kim, Y.C.J.C.P.B.E. Jung, Rapidly self-heating shape memory polyurethane nanocomposite with boron-doped single-walled carbon nanotubes using near-infrared laser, 175 (2019) 107065.
[13] W. Du, Y. Jin, S. Lai, L. Shi, W. Fan, J.J.P. Pan, Near-infrared light triggered shape memory and self-healable polyurethane/functionalized graphene oxide composites containing diselenide bonds, 158 (2018) 120-129.
[14] Y. Zhang, J. Hu, S. Zhu, T. Qin, F.J.C.S. Ji, Technology, A “trampoline” nanocomposite: Tuning the interlayer spacing in graphene oxide/polyurethane to achieve coalesced mechanical and memory properties, 180 (2019) 14-22.
[15] H.J. Yoo, B.H. Lee, S.S. Mahapatra, C.-M. Yang, J.W.J.J.o.A.P.S. Cho, Polyurethane nanocomposites with click-coupled nanodiamonds exhibiting enhanced mechanical and shape memory effects, 134(43) (2017) 45465.
[16] S. Ghotia, A. Kumar, V. Sudarsan, N. Dwivedi, S. Singh, P. Kumar, Multilayered Ti3C2Tx MXenes: A prominent materials for hydrogen storage, International Journal of Hydrogen Energy (2023). https://doi.org/https://doi.org/10.1016/j.ijhydene.2023.05.145.
[17] S. Kumar, N. Kumari, Y. Seo, MXenes: Versatile 2D materials with tailored surface chemistry and diverse applications, Journal of Energy Chemistry 90 (2024) 253-293. https://doi.org/https://doi.org/10.1016/j.jechem.2023.11.031.
[18] L. Jia, S. Zhou, A. Ahmed, Z. Yang, S. Liu, H. Wang, F. Li, M. Zhang, Y. Zhang, L. Sun, Tuning MXene electrical conductivity towards multifunctionality, Chemical Engineering Journal 475 (2023) 146361. https://doi.org/https://doi.org/10.1016/j.cej.2023.146361.

[19] V.-H. Nguyen, B.-S. Nguyen, C. Hu, C.C. Nguyen, D.L.T. Nguyen, M.T. Nguyen Dinh, D.-V.N. Vo, Q.T. Trinh, M. Shokouhimehr, A. Hasani, Novel architecture titanium carbide (Ti3C2Tx) MXene cocatalysts toward photocatalytic hydrogen production: a mini-review, Nanomaterials 10(4) (2020) 602.
[20] J. Björk, J. Rosen, Functionalizing MXenes by Tailoring Surface Terminations in Different Chemical Environments, Chemistry of Materials 33(23) (2021) 9108-9118. https://doi.org/10.1021/acs.chemmater.1c01264.
[21] S. Nema, M. Patel, S. Jaiswal, C. Dhand, N. Dwivedi, Polydopamine Modified Ti3AlC2 MAX Phase Promotes Electrochemical Heavy Metal Detection, Surfaces and Interfaces (2024) 104752.
[22] K. Chen, N. Qiu, Q. Deng, M.-H. Kang, H. Yang, J.-U. Baek, Y.-H. Koh, S. Du, Q. Huang, H.-E. Kim, Cytocompatibility of Ti3AlC2, Ti3SiC2, and Ti2AlN: In Vitro Tests and First-Principles Calculations, ACS Biomaterials Science & Engineering 3(10) (2017) 2293-2301. https://doi.org/10.1021/acsbiomaterials.7b00432.
[23] K.H. Tan, L. Samylingam, N. Aslfattahi, R. Saidur, K. Kadirgama, Optical and conductivity studies of polyvinyl alcohol-MXene (PVA-MXene) nanocomposite thin films for electronic applications, Optics & Laser Technology 136 (2021) 106772. https://doi.org/https://doi.org/10.1016/j.optlastec.2020.106772.
[24] Z. Jia, Z. Li, S. Ma, W. Zhang, Y. Chen, Y. Luo, D. Jia, B. Zhong, J.M. Razal, X.J.J.o.C. Wang, I. Science, Constructing conductive titanium carbide nanosheet (MXene) network on polyurethane/polyacrylonitrile fibre framework for flexible strain sensor, 584 (2021) 1-10.
[25] Z. Chi, C. Wang, Y. Dong, Y. Zhou, H. Xu, Z. Islam, C. Qian, Y. Fu, MXene/epoxy-based shape memory nanocomposites with highly stable thermal-mechanical coupling effect for constructing an effective information transmission medium, Composites Science and Technology 225 (2022) 109505.
[26] P. Srinivas, L. Jacob, M. Shebeeb C, H. Butt, I. Barsoum, R.K. Abu Al-Rub, W. Zaki, Mechanical Properties, Energy Absorption, and Shape Memory Behavior of 3D Printed PLA-MXene Nanocomposites and Gyroid Lattices, Advanced Engineering Materials (2024) 2301698.
[27] M. Naguib, M.W. Barsoum, Y.J.A.M. Gogotsi, Ten years of progress in the synthesis and development of MXenes, 33(39) (2021) 2103393.
[28] N. Bisht, M. Patel, N. Dwivedi, P. Kumar, D.P. Mondal, A.K. Srivastava, C. Dhand, Bio-inspired polynorepinephrine based nanocoatings for reduced graphene oxide/gold nanoparticles composite for high-performance biosensing of Mycobacterium tuberculosis, Environmental Research 227 (2023) 115684. https://doi.org/https://doi.org/10.1016/j.envres.2023.115684.
[29] S. Ghotia, T. Rimza, S. Singh, N. Dwivedi, A.K. Srivastava, P. Kumar, Hetero-atom doped graphene for marvellous hydrogen storage: unveiling recent advances and future pathways, Journal of Materials Chemistry A 12(21) (2024) 12325-12357. https://doi.org/10.1039/D4TA00717D.
[30] B. Anasori, M.R. Lukatskaya, Y.J.N.R.M. Gogotsi, 2D metal carbides and nitrides (MXenes) for energy storage, 2(2) (2017) 1-17.
[31] Y. Gogotsi, B.J.A.n. Anasori, The rise of MXenes, ACS Publications, 2019, pp. 8491-8494.
[32] B. Anasori, Y. Xie, M. Beidaghi, J. Lu, B.C. Hosler, L. Hultman, P.R. Kent, Y. Gogotsi, M.W.J.A.n. Barsoum, Two-dimensional, ordered, double transition metals carbides (MXenes), 9(10) (2015) 9507-9516.
[33] M. Malaki, X. Jiang, H. Wang, R. Podila, H. Zhang, P. Samorì, R.S.J.C.E.J. Varma, MXenes: from past to future perspectives, 463 (2023) 142351.
[34] B. Anasori, M. Dahlqvist, J. Halim, E.J. Moon, J. Lu, B. Hosler, E.a. Caspi, S. May, L. Hultman, P. Eklund, J. Rosén, M. Barsoum, Experimental and theoretical characterization of ordered MAX phases Mo2TiAlC2 and Mo2Ti2AlC3, Journal of Applied Physics 118 (2015) 94304-7. https://doi.org/10.1063/1.4929640.
[35] M. Li, J. Lu, K. Luo, Y. Li, K. Chang, K. Chen, J. Zhou, J. Rosen, L. Hultman, P. Eklund, P.O.Å. Persson, S. Du, Z. Chai, Z. Huang, Q. Huang, Element Replacement Approach by Reaction with Lewis Acidic Molten Salts to Synthesize Nanolaminated MAX Phases and MXenes, Journal of the American Chemical Society 141(11) (2019) 4730-4737. https://doi.org/10.1021/jacs.9b00574.
[36] Y. Gogotsi, Q. Huang, MXenes: Two-Dimensional Building Blocks for Future Materials and Devices, ACS Nano 15(4) (2021) 5775-5780. https://doi.org/10.1021/acsnano.1c03161.
[37] F. Ming, H. Liang, G. Huang, Z. Bayhan, H.N. Alshareef, MXenes for rechargeable batteries beyond the lithium-ion, Advanced Materials 33(1) (2021) 2004039.

[38] M.R. Lukatskaya, O. Mashtalir, C.E. Ren, Y. Dall'Agnese, P. Rozier, P.L. Taberna, M. Naguib, P. Simon, M.W. Barsoum, Y. Gogotsi, Cation intercalation and high volumetric capacitance of two-dimensional titanium carbide, Science 341(6153) (2013) 1502-1505.
[39] M. Naguib, M. Barsoum, Y. Gogotsi, Ten Years of Progress in the Synthesis and Development of MXenes, Advanced Materials 33 (2021) 2103393. https://doi.org/10.1002/adma.202103393.
[40] C.C. Hornat, Y. Yang, M.W.J.A.M. Urban, Quantitative predictions of shape-memory effects in polymers, 29(7) (2017) 1603334.
[41] K. McLellan, T. Li, Y.-C. Sun, M.B. Jakubinek, H.E.J.A.A.P.M. Naguib, 4D Printing of MXene Composites for Deployable Actuating Structures, 4(12) (2022) 8774-8785.
[42] Q. Zhao, H.J. Qi, T.J.P.i.P.S. Xie, Recent progress in shape memory polymer: New behavior, enabling materials, and mechanistic understanding, 49 (2015) 79-120.
[43] L.C. Chang, T.J.J. Read, Plastic deformation and diffusionless phase changes in metals—The gold-cadmium beta phase, 3 (1951) 47-52.
[44] W.M. Huang, Z. Ding, C.C. Wang, J. Wei, Y. Zhao, H. Purnawali, Shape memory materials, Materials Today 13(7) (2010) 54-61. https://doi.org/https://doi.org/10.1016/S1369-7021(10)70128-0.
[45] L.B. Vernon, H.M. Vernon, Process of manufacturing articles of thermoplastic synthetic resins, Google Patents, 1941.
[46] C. Liu, H. Qin, P.T. Mather, Review of progress in shape-memory polymers, Journal of Materials Chemistry 17(16) (2007) 1543-1558. https://doi.org/10.1039/B615954K.
[47] D. Ratna, J. Karger-Kocsis, Recent advances in shape memory polymers and composites: a review, Journal of Materials Science 43 (2007) 254-269. https://doi.org/10.1007/s10853-007-2176-7.
[48] M. Carey, M.J.M.T.A. Barsoum, MXene polymer nanocomposites: A review, 9 (2021) 100120.
[49] H. Riazi, S.K. Nemani, M.C. Grady, B. Anasori, M.J.J.o.M.C.A. Soroush, Ti 3 C 2 MXene–polymer nanocomposites and their applications, 9(13) (2021) 8051-8098.
[50] K. Gong, K. Zhou, X. Qian, C. Shi, B.J.C.P.B.E. Yu, MXene as emerging nanofillers for high-performance polymer composites: A review, 217 (2021) 108867.
[51] L. Li, X. Liu, J. Wang, Y. Yang, Y. Cao, W.J.C.P.A.A.S. Wang, Manufacturing, New application of MXene in polymer composites toward remarkable anti-dripping performance for flame retardancy, 127 (2019) 105649.
[52] Y. Pan, L. Fu, Q. Zhou, Z. Wen, C.T. Lin, J. Yu, W. Wang, H.J.P.C. Zhao, Flammability, thermal stability and mechanical properties of polyvinyl alcohol nanocomposites reinforced with delaminated Ti3C2Tx (MXene), 41(1) (2020) 210-218.
[53] X. Wang, L. Wang, Y. He, M. Wu, A.J.P.C. Zhou, The effect of two-dimensional d-Ti3C2 on the mechanical and thermal conductivity properties of thermoplastic polyurethane composites, 41(1) (2020) 350-359.
[54] B. Yu, B. Tawiah, L.-Q. Wang, A.C.Y. Yuen, Z.-C. Zhang, L.-L. Shen, B. Lin, B. Fei, W. Yang, A.J.J.o.h.m. Li, Interface decoration of exfoliated MXene ultra-thin nanosheets for fire and smoke suppressions of thermoplastic polyurethane elastomer, 374 (2019) 110-119.
[55] L. Ma, M. Hamidinejad, C. Liang, B. Zhao, S. Habibpour, A. Yu, T. Filleter, C.B.J.C. Park, Enhanced electromagnetic wave absorption performance of polymer/SiC-nanowire/MXene (Ti3C2Tx) composites, 179 (2021) 408-416.
[56] K. Rajavel, S. Luo, Y. Wan, X. Yu, Y. Hu, P. Zhu, R. Sun, C.J.C.P.A.A.S. Wong, Manufacturing, 2D Ti3C2Tx MXene/polyvinylidene fluoride (PVDF) nanocomposites for attenuation of electromagnetic radiation with excellent heat dissipation, 129 (2020) 105693.
[57] G. Song, R. Kang, L. Guo, Z. Ali, X. Chen, Z. Zhang, C. Yan, C.-T. Lin, N. Jiang, J.J.N.J.o.C. Yu, Highly flexible few-layer Ti 3 C 2 MXene/cellulose nanofiber heat-spreader films with enhanced thermal conductivity, 44(17) (2020) 7186-7193.
[58] Z. Liu, W. Wang, J. Tan, J. Liu, M. Zhu, B. Zhu, Q.J.J.o.M.C.C. Zhang, Bioinspired ultra-thin polyurethane/MXene nacre-like nanocomposite films with synergistic mechanical properties for electromagnetic interference shielding, 8(21) (2020) 7170-7180.
[59] X. Chen, Y. Zhao, L. Li, Y. Wang, J. Wang, J. Xiong, S. Du, P. Zhang, X. Shi, J.J.P.R. Yu, MXene/polymer nanocomposites: preparation, properties, and applications, 61(1) (2021) 80-115.

[60] S. He, X. Sun, H. Zhang, C. Yuan, Y. Wei, J.J.M.R.C. Li, Preparation strategies and applications of MXene-polymer composites: a review, 42(19) (2021) 2100324.
[61] X. Lu, J. Zhu, W. Wu, B. Zhang, Hierarchical architecture of PANI@TiO2/Ti3C2Tx ternary composite electrode for enhanced electrochemical performance, Electrochimica Acta 228 (2017) 282-289. https://doi.org/https://doi.org/10.1016/j.electacta.2017.01.025.
[62] P. Zhang, X.-J. Yang, P. Li, Y. Zhao, Q.J.J.S.M. Niu, Fabrication of novel MXene (Ti 3 C 2)/polyacrylamide nanocomposite hydrogels with enhanced mechanical and drug release properties, 16(1) (2020) 162-169.
[63] L. Tong, C. Jiang, K. Cai, P.J.J.o.P.S. Wei, High-performance and freestanding PPy/Ti3C2Tx composite film for flexible all-solid-state supercapacitors, 465 (2020) 228267.
[64] L. Wang, P. Song, C.-T. Lin, J. Kong, J.J.R. Gu, 3D shapeable, superior electrically conductive cellulose nanofibers/Ti3C2Tx MXene aerogels/epoxy nanocomposites for promising EMI shielding, (2020).
[65] L. Wang, H. Qiu, P. Song, Y. Zhang, Y. Lu, C. Liang, J. Kong, L. Chen, J.J.C.P.A.A.S. Gu, Manufacturing, 3D Ti3C2Tx MXene/C hybrid foam/epoxy nanocomposites with superior electromagnetic interference shielding performances and robust mechanical properties, 123 (2019) 293-300.
[66] H. Zhang, L. Wang, Q. Chen, P. Li, A. Zhou, X. Cao, Q.J.M. Hu, Design, Preparation, mechanical and anti-friction performance of MXene/polymer composites, 92 (2016) 682-689.
[67] Y. Shi, C. Liu, L. Liu, L. Fu, B. Yu, Y. Lv, F. Yang, P.J.C.E.J. Song, Strengthening, toughing and thermally stable ultra-thin MXene nanosheets/polypropylene nanocomposites via nanoconfinement, 378 (2019) 122267.
[68] X. Sheng, Y. Zhao, L. Zhang, X.J.C.S. Lu, Technology, Properties of two-dimensional Ti3C2 MXene/thermoplastic polyurethane nanocomposites with effective reinforcement via melt blending, 181 (2019) 107710.
[69] B. Lin, A.C.Y. Yuen, A. Li, Y. Zhang, T.B.Y. Chen, B. Yu, E.W.M. Lee, S. Peng, W. Yang, H.-D.J.J.o.h.m. Lu, MXene/chitosan nanocoating for flexible polyurethane foam towards remarkable fire hazards reductions, 381 (2020) 120952.
[70] Y. Huang, S. Jiang, R. Liang, P. Sun, Y. Hai, L.J.C.E.J. Zhang, Thermal-triggered insulating fireproof layers: A novel fire-extinguishing MXene composites coating, 391 (2020) 123621.
[71] X.-P. Li, Y. Li, X. Li, D. Song, P. Min, C. Hu, H.-B. Zhang, N. Koratkar, Z.-Z.J.J.o.c. Yu, i. science, Highly sensitive, reliable and flexible piezoresistive pressure sensors featuring polyurethane sponge coated with MXene sheets, 542 (2019) 54-62.
[72] Q.W. Wang, H.B. Zhang, J. Liu, S. Zhao, X. Xie, L. Liu, R. Yang, N. Koratkar, Z.Z.J.A.F.M. Yu, Multifunctional and water-resistant MXene-decorated polyester textiles with outstanding electromagnetic interference shielding and joule heating performances, 29(7) (2019) 1806819.
[73] N. Kumar, H. Singh, M. Khatri, N. Bhardwaj, 2D-Transition Metal Carbides and Nitrides: Materials for the Next Generation, Age of MXenes, Volume 1. Fundamentals and Artificial Intelligence: Machine Learning Interventions, American Chemical Society2023, pp. 1-25. https://doi.org/doi:10.1021/bk-2023-1442.ch001

10.1021/bk-2023-1442.ch001.
[74] S. Ghotia, A. Kumar, V. Sudarsan, N. Dwivedi, S. Singh, P. Kumar, Multilayered Ti3C2Tx MXenes: A prominent materials for hydrogen storage, International Journal of Hydrogen Energy 52 (2024) 100-107. https://doi.org/https://doi.org/10.1016/j.ijhydene.2023.05.145.
[75] X. Qi, Y. Dong, M.D.Z. Islam, Y. Zhu, Y. Fu, S.-Y. Fu, Excellent triple-shape memory effect and superior recovery stress of ethylene-vinyl acetate copolymer fiber, Composites Science and Technology 203 (2021) 108609. https://doi.org/https://doi.org/10.1016/j.compscitech.2020.108609.
[76] L. Yu, L. Lu, X. Zhou, L. Xu, Current understanding of the wettability of MXenes, Advanced Materials Interfaces 10(2) (2023) 2201818.
[77] H. Zhang, L. Wang, Q. Chen, P. Li, A. Zhou, X. Cao, Q. Hu, Preparation, mechanical and anti-friction performance of MXene/polymer composites, Materials & Design 92 (2016) 682-689.
[78] H. Zhang, L. Wang, A. Zhou, C. Shen, Y. Dai, F. Liu, J. Chen, P. Li, Q. Hu, Effects of 2-D transition metal carbide Ti 2 CT x on properties of epoxy composites, RSC advances 6(90) (2016) 87341-87352.
[79] P. Das, P.K. Marvi, S. Ganguly, X. Tang, B. Wang, S. Srinivasan, A.R. Rajabzadeh, A. Rosenkranz, MXene-Based Elastomer Mimetic Stretchable Sensors: Design, Properties, and Applications, Nano-Micro Letters 16(1) (2024) 135. https://doi.org/10.1007/s40820-024-01349-w.

[80] R. Sanaka, S.K. Sahu, Experimental investigation into mechanical, thermal, and shape memory behavior of thermoresponsive PU/MXene shape memory polymer nanocomposite, Heliyon 10(2) (2024).
[81] Q. Li, H. He, X. Ye, F. Guan, Y. Ai, Y. Shen, C. Zhang, NIR light-induced functionalized MXene as a dynamic-crosslinker for reinforced polyurethane composites with shape memory and self-healing, Chemical Engineering Journal 475 (2023) 146500.
[82] J. Zhang, N. Kong, S. Uzun, A. Levitt, S. Seyedin, P.A. Lynch, S. Qin, M. Han, W. Yang, J. Liu, Scalable manufacturing of free-standing, strong Ti3C2Tx MXene films with outstanding conductivity, Advanced Materials 32(23) (2020) 2001093.
[83] S. Gao, J. Ding, W. Wang, J. Lu, MXene based flexible composite phase change material with shape memory, self-healing and flame retardant for thermal management, Composites Science and Technology 234 (2023) 109945. https://doi.org/https://doi.org/10.1016/j.compscitech.2023.109945.
[84] S. Jaiswal, J. Vishwakarma, S. Bhatt, S. Karak, P. Bharti, C. Dhand, R. Kumar, P. Kumar, M.S. Saifullah, S. Saha, Layered Titanium Carbide-Mediated Fast Shape Switching and Excellent Thermal and Electrical Transport in Shape-Memory-Polymer Composites for Smart Technologies: MAX Versus MXene, Advanced Engineering Materials 25(17) (2023) 2300233.
[85] M. Xie, S. Li, X. Qi, Z. Chi, L. Shen, Z. Islam, Y. Dong, Thermal and infrared light self-repairing, high sensitivity, and large strain sensing range shape memory MXene/CNTs/EVA composites fiber strain sensor for human motion monitoring, Sensors and Actuators A: Physical 347 (2022) 113939. https://doi.org/https://doi.org/10.1016/j.sna.2022.113939.
[86] J. Chen, W.-j. Jiang, Z. Zeng, D.-x. Sun, X.-d. Qi, J.-h. Yang, Y. Wang, Multifunctional shape memory foam composites integrated with tunable electromagnetic interference shielding and sensing, Chemical Engineering Journal 466 (2023) 143373.
[87] X. Zhan, C. Si, J. Zhou, Z. Sun, MXene and MXene-based composites: synthesis, properties and environment-related applications, Nanoscale Horizons 5(2) (2020) 235-258.
[88] A. Lipatov, M. Alhabeb, M.R. Lukatskaya, A. Boson, Y. Gogotsi, A. Sinitskii, Effect of synthesis on quality, electronic properties and environmental stability of individual monolayer Ti3C2 MXene flakes, Advanced Electronic Materials 2(12) (2016) 1600255.
[89] R.M. Ronchi, J.T. Arantes, S.F. Santos, Synthesis, structure, properties and applications of MXenes: Current status and perspectives, Ceramics International 45(15) (2019) 18167-18188.
[90] X. Tang, X. Guo, W. Wu, G. Wang, 2D metal carbides and nitrides (MXenes) as high-performance electrode materials for Lithium-based batteries, Advanced Energy Materials 8(33) (2018) 1801897.
[91] A.S. Zeraati, S.A. Mirkhani, P. Sun, M. Naguib, P.V. Braun, U. Sundararaj, Improved synthesis of Ti 3 C 2 T x MXenes resulting in exceptional electrical conductivity, high synthesis yield, and enhanced capacitance, Nanoscale 13(6) (2021) 3572-3580.
[92] X. Zang, J. Wang, Y. Qin, T. Wang, C. He, Q. Shao, H. Zhu, N. Cao, Enhancing capacitance performance of Ti 3 C 2 T x MXene as electrode materials of supercapacitor: from controlled preparation to composite structure construction, Nano-Micro Letters 12 (2020) 1-24.
[93] M. Han, C.E. Shuck, R. Rakhmanov, D. Parchment, B. Anasori, C.M. Koo, G. Friedman, Y. Gogotsi, Beyond Ti3C2T x: MXenes for electromagnetic interference shielding, ACS nano 14(4) (2020) 5008-5016.
[94] H. Kim, B. Anasori, Y. Gogotsi, H.N. Alshareef, Thermoelectric properties of two-dimensional molybdenum-based MXenes, Chemistry of Materials 29(15) (2017) 6472-6479.
[95] J. Yan, C.E. Ren, K. Maleski, C.B. Hatter, B. Anasori, P. Urbankowski, A. Sarycheva, Y. Gogotsi, Flexible MXene/graphene films for ultrafast supercapacitors with outstanding volumetric capacitance, Advanced Functional Materials 27(30) (2017) 1701264.
[96] A. Feng, T. Hou, Z. Jia, Y. Zhang, F. Zhang, G.J.N. Wu, Preparation and characterization of epoxy resin filled with Ti3C2Tx MXene nanosheets with excellent electric conductivity, 10(1) (2020) 162.
[97] L. Wang, H. Qiu, P. Song, Y. Zhang, Y. Lu, C. Liang, J. Kong, L. Chen, J. Gu, 3D Ti3C2Tx MXene/C hybrid foam/epoxy nanocomposites with superior electromagnetic interference shielding performances and robust mechanical properties, Composites Part A: Applied Science and Manufacturing 123 (2019) 293-300.

[98] X. Jin, J. Wang, L. Dai, X. Liu, L. Li, Y. Yang, Y. Cao, W. Wang, H. Wu, S.J.C.E.J. Guo, Flame-retardant poly (vinyl alcohol)/MXene multilayered films with outstanding electromagnetic interference shielding and thermal conductive performances, 380 (2020) 122475.
[99] J. Lu, Y. Zhang, Y. Tao, B. Wang, W. Cheng, G. Jie, L. Song, Y. Hu, Self-healable castor oil-based waterborne polyurethane/MXene film with outstanding electromagnetic interference shielding effectiveness and excellent shape memory performance, Journal of Colloid and Interface Science 588 (2021) 164-174. https://doi.org/https://doi.org/10.1016/j.jcis.2020.12.076.
[100] Y.-j. He, Y.-w. Shao, Y.-y. Xiao, J.-h. Yang, X.-d. Qi, Y. Wang, Multifunctional phase change composites based on elastic MXene/silver nanowire sponges for excellent thermal/solar/electric energy storage, shape memory, and adjustable electromagnetic interference shielding functions, ACS Applied Materials & Interfaces 14(4) (2022) 6057-6070.
[101] S. Jaiswal, J. Vishwakarma, S. Bhatt, S. Karak, P. Bharti, C. Dhand, R. Kumar, P. Kumar, M.S.M. Saifullah, S. Saha, R. Mishra, N. Dwivedi, Layered Titanium Carbide-Mediated Fast Shape Switching and Excellent Thermal and Electrical Transport in Shape-Memory-Polymer Composites for Smart Technologies: MAX Versus MXene, Advanced Engineering Materials n/a(n/a) 2300233. https://doi.org/https://doi.org/10.1002/adem.202300233.
[102] L. He, J. Wang, B. Wang, X. Wang, X. Zhou, W. Cai, X. Mu, Y. Hou, Y. Hu, L. Song, Large-scale production of simultaneously exfoliated and Functionalized Mxenes as promising flame retardant for polyurethane, Composites Part B: Engineering 179 (2019) 107486.
[103] R. Kang, Z. Zhang, L. Guo, J. Cui, Y. Chen, X. Hou, B. Wang, C.-T. Lin, N. Jiang, J.J.S.r. Yu, Enhanced thermal conductivity of epoxy composites filled with 2D transition metal carbides (MXenes) with ultralow loading, 9(1) (2019) 9135.
[104] J. Zhang, N. Kong, S. Uzun, A. Levitt, S. Seyedin, P.A. Lynch, S. Qin, M. Han, W. Yang, J.J.A.M. Liu, Scalable manufacturing of free-standing, strong Ti3C2Tx MXene films with outstanding conductivity, 32(23) (2020) 2001093.
[105] F. Luo, K. Wu, H. Guo, Q. Zhao, M.J.P.I. Lu, Simultaneous reduction and surface functionalization of graphene oxide for enhancing flame retardancy and thermal conductivity of mesogenic epoxy composites, 66(1) (2017) 98-107.
[106] X. Huang, C. Zhi, Y. Lin, H. Bao, G. Wu, P. Jiang, Y.-W.J.M.S. Mai, E.R. Reports, Thermal conductivity of graphene-based polymer nanocomposites, 142 (2020) 100577.
[107] D. Wang, Y. Lin, D. Hu, P. Jiang, X. Huang, Multifunctional 3D-MXene/PDMS nanocomposites for electrical, thermal and triboelectric applications, Composites Part A: Applied Science and Manufacturing 130 (2020) 105754. https://doi.org/https://doi.org/10.1016/j.compositesa.2019.105754.
[108] L. Li, X. Liu, J. Wang, Y. Yang, Y. Cao, W. Wang, New application of MXene in polymer composites toward remarkable anti-dripping performance for flame retardancy, Composites Part A: Applied Science and Manufacturing 127 (2019) 105649.
[109] D. Ratna, J.J.J.o.M.S. Karger-Kocsis, Recent advances in shape memory polymers and composites: a review, 43 (2008) 254-269.
[110] A. Lendlein, S. Kelch, Shape-Memory Polymers, Angewandte Chemie International Edition 41(12) (2002) 2034-2057. https://doi.org/https://doi.org/10.1002/1521-3773(20020617)41:12<2034::AID-ANIE2034>3.0.CO;2-M.
[111] H.Y. Jiang, S. Kelch, A. Lendlein, Polymers Move in Response to Light, Advanced Materials 18(11) (2006) 1471-1475. https://doi.org/https://doi.org/10.1002/adma.200502266.
[112] M. Behl, A. Lendlein, Shape-memory polymers, Materials today 10(4) (2007) 20-28.
[113] J. Morshedian, H.A. Khonakdar, S. Rasouli, Modeling of Shape Memory Induction and Recovery in Heat-Shrinkable Polymers, Macromolecular Theory and Simulations 14(7) (2005) 428-434. https://doi.org/https://doi.org/10.1002/mats.200400108.
[114] G. Barot, I.J. Rao, Constitutive modeling of the mechanics associated with crystallizable shape memory polymers, Zeitschrift für angewandte Mathematik und Physik ZAMP 57(4) (2006) 652-681. https://doi.org/10.1007/s00033-005-0009-6.

[115] W. Wang, T. Cai, Z. Cheng, Y. Yang, J. Wang, J. Tang, L. Tang, W. Feng, Y. Liu, Z. Fan, A shape programmable MXene-based supermolecular nanocomposite film, Composites Part A: Applied Science and Manufacturing 159 (2022) 106997.
[116] Y. Dong, Y. Yin, X. Du, C. Liu, Q. Zhou, Effect of MXene@ PANI on the self-healing property of shape memory-assisted coating, Synthetic Metals 291 (2022) 117162.
[117] L. Zhang, Y. Huang, H. Dong, R. Xu, S. Jiang, Flame-retardant shape memory polyurethane/MXene paper and the application for early fire alarm sensor, Composites Part B: Engineering 223 (2021) 109149. https://doi.org/10.1016/j.compositesb.2021.109149.
[118] K. McLellan, T. Li, Y.-C. Sun, M.B. Jakubinek, H.E. Naguib, 4D printing of MXene composites for deployable actuating structures, ACS Applied Polymer Materials 4(12) (2022) 8774-8785.
[119] W. Wang, T. Cai, L. Tang, J. Zhang, C. Du, J. Tang, Y. Yang, L. Yin, H. Kang, Z. Fan, Shape-Reconfigurable Supramolecular MXene-Based Memory Films, ACS Applied Nano Materials 6(20) (2023) 18721-18728.
[120] X.-R. Guo, P.-H. Sheng, J.-W. Hu, J. Liu, S.-L. Wang, Q. Ma, Z.-Z. Yu, Y. Ding, Multistimuli-Responsive Shape-Memory Composites with a Water-Assisted Self-Healing Function Based on Sodium Carboxymethyl Cellulose/Poly (vinyl alcohol)/MXene, ACS Applied Materials & Interfaces 16(14) (2024) 17981-17991.
[121] J. Hu, J. Xie, T. Peng, Q. Shi, C. Pan, H. Tan, J. Sun, Fabrication of a MXene-based shape-memory hydrogel and its application in the wound repair of skin, Soft Matter 20(20) (2024) 4136-4142.
[122] H. Ur Rehman, Y. Chen, M.S. Hedenqvist, H. Li, W. Xue, Y. Guo, Y. Guo, H. Duan, H. Liu, Self-healing shape memory PUPCL copolymer with high cycle life, Advanced Functional Materials 28(7) (2018) 1704109.
[123] Y. Deng, F. Zhang, Y. Liu, S. Zhang, H. Yuan, J. Leng, 4D printed shape memory polyurethane-based composite for bionic cartilage scaffolds, ACS Applied Polymer Materials 5(2) (2023) 1283-1292.
[124] C. Yue, M. Hua, H. Li, Y. Liu, M. Xu, Y. Song, Printability, shape-memory, and mechanical properties of PHB/PCL/CNFs composites, Journal of Applied Polymer Science 138(22) (2021) 50510.
[125] Y.-j. He, Y.-w. Shao, Y.-y. Xiao, J.-h. Yang, X.-d. Qi, Y.J.A.A.M. Wang, Interfaces, Multifunctional phase change composites based on elastic MXene/silver nanowire sponges for excellent thermal/solar/electric energy storage, shape memory, and adjustable electromagnetic interference shielding functions, 14(4) (2022) 6057-6070.
[126] R. Bayan, N. Karak, Renewable resource derived aliphatic hyperbranched polyurethane/aluminium hydroxide–reduced graphene oxide nanocomposites as robust, thermostable material with multi-stimuli responsive shape memory features, New Journal of Chemistry 41(17) (2017) 8781-8790.
[127] Y. Dong, Y. Yin, X. Du, C. Liu, Q.J.S.M. Zhou, Effect of MXene@ PANI on the self-healing property of shape memory-assisted coating, 291 (2022) 117162.
[128] W.-w. Hu, X.-y. Shi, M.-h. Gao, C.-h. Huang, T. Huang, N. Zhang, J.-h. Yang, X.-d. Qi, Y. Wang, Light-actuated shape memory and self-healing phase change composites supported by MXene/waterborne polyurethane aerogel for superior solar-thermal energy storage, Composites Communications 28 (2021) 100980.
[129] J. Lu, Y. Zhang, Y. Tao, B. Wang, W. Cheng, G. Jie, L. Song, Y.J.J.o.C. Hu, I. Science, Self-healable castor oil-based waterborne polyurethane/MXene film with outstanding electromagnetic interference shielding effectiveness and excellent shape memory performance, 588 (2021) 164-174.
[130] J. Hu, S. Li, J. Zhang, Q. Chang, W. Yu, Y.J.C.C.L. Zhou, Mechanical properties and frictional resistance of Al composites reinforced with Ti3C2Tx MXene, 31(4) (2020) 996-999.
[131] K.L. Firestein, J.E. von Treifeldt, D.G. Kvashnin, J.F. Fernando, C. Zhang, A.G. Kvashnin, E.V. Podryabinkin, A.V. Shapeev, D.P. Siriwardena, P.B.J.N.L. Sorokin, Young's modulus and tensile strength of Ti3C2 MXene nanosheets as revealed by in situ TEM probing, AFM nanomechanical mapping, and theoretical calculations, 20(8) (2020) 5900-5908.
[132] Y. Hai, S. Jiang, C. Zhou, P. Sun, Y. Huang, S.J.D.T. Niu, Fire-safe unsaturated polyester resin nanocomposites based on MAX and MXene: A comparative investigation of their properties and mechanism of fire retardancy, 49(18) (2020) 5803-5814.
[133] L. Liu, J. Feng, Y. Xue, V. Chevali, Y. Zhang, Y. Shi, L.C. Tang, P.J.A.F.M. Song, 2D MXenes for Fire Retardancy and Fire-Warning Applications: Promises and Prospects, 33(9) (2023) 2212124.

[134] C. Jiang, J. Chen, X. Lai, H. Li, X. Zeng, Y. Zhao, Q. Zeng, J. Gao, Z. Wu, Y. Qiu, Mechanically robust and multifunctional polyimide/MXene composite aerogel for smart fire protection, Chemical Engineering Journal 434 (2022) 134630. https://doi.org/https://doi.org/10.1016/j.cej.2022.134630.
[135] Y. Zhao, J. Chen, X. Lai, H. Li, X. Zeng, C. Jiang, Q. Zeng, K. Li, Z. Wu, Y. Qiu, Efficient flame-retardant and multifunctional polyimide/MXene composite aerogel for intelligent fire protection, Composites Part A: Applied Science and Manufacturing 163 (2022) 107210. https://doi.org/https://doi.org/10.1016/j.compositesa.2022.107210.
[136] T. Ma, L. Li, M. Pan, C. Guo, C. Mei, Multifunctional MXene-based fire alarm wallpaper with sandwich-like structure for enhanced fire safety and prevention, Chemical Engineering Journal 451 (2023) 138517. https://doi.org/https://doi.org/10.1016/j.cej.2022.138517.
[137] W. Liu, X. Wang, Y. Song, R. Cao, L. Wang, Z. Yan, G.J.N.E. Shan, Self-powered forest fire alarm system based on impedance matching effect between triboelectric nanogenerator and thermosensitive sensor, 73 (2020) 104843.
[138] L. Zhang, Y. Huang, H. Dong, R. Xu, S.J.C.P.B.E. Jiang, Flame-retardant shape memory polyurethane/MXene paper and the application for early fire alarm sensor, 223 (2021) 109149.
[139] W. Yang, W. Zhou, N. Ding, S. Shen, D. Gao, D. Puglia, Y. Duan, X. Pengwu, T. Liu, Z. Wang, Biobased Photothermal Responsive Shape Memory Polythioether/Mxene Nanocomposites with Self-Extinguishing Performance, Mxene Nanocomposites with Self-Extinguishing Performance.
[140] G. Scalet, Two-way and multiple-way shape memory polymers for soft robotics: An overview, Actuators, MDPI, 2020, p. 10.
[141] Z. Shen, F. Chen, X. Zhu, K.-T. Yong, G.J.J.o.M.C.B. Gu, Stimuli-responsive functional materials for soft robotics, 8(39) (2020) 8972-8991.
[142] X. Zhang, R. Nie, Y. Chen, B.J.J.o.E. He, Deployable structures: structural design and static/dynamic analysis, (2021) 1-37.
[143] Z.-Q. Liu, H. Qiu, X. Li, S.-L.J.C.J.o.M.E. Yang, Review of large spacecraft deployable membrane antenna structures, 30(6) (2017) 1447-1459.
[144] X. Wang, Y. He, J. Leng, Bionic Shape Memory Polyurethane/Prussian Blue Nanoparticle-Based Actuators with Two-Way and Programmable Light-Driven Motions, ACS Applied Polymer Materials 5(2) (2023) 1398-1408. https://doi.org/10.1021/acsapm.2c01911.
[145] S. Sarrafan, X. Feng, G. Li, A soft syntactic foam actuator with high recovery stress, actuation strain, and energy output, Materials Today Communications 31 (2022) 103303. https://doi.org/https://doi.org/10.1016/j.mtcomm.2022.103303.
[146] X. Wei, H. Li, X. He, Z. Li, H. Ye, W. Xue, Q. Ge, Shape Memory Polymer-based Stiffness Variable Soft Actuator Via Digital Light Processing-based 3D Printing, 2021 27th International Conference on Mechatronics and Machine Vision in Practice (M2VIP), 2021, pp. 612-616.
[147] J.J. Song, H.H. Chang, H.E.J.E.P.J. Naguib, Biocompatible shape memory polymer actuators with high force capabilities, 67 (2015) 186-198.
[148] W. Wang, Y. Liu, J.J.C.C.R. Leng, Recent developments in shape memory polymer nanocomposites: Actuation methods and mechanisms, 320 (2016) 38-52.
[149] W. Liu, H. Chen, M. Ge, Q.-Q. Ni, Q. Gao, Electroactive shape memory composites with TiO2 whiskers for switching an electrical circuit, Materials & Design 143 (2018) 196-203.
[150] Z.-x. Zhang, W.-y. Wang, J.-h. Yang, N. Zhang, T. Huang, Y. Wang, Excellent Electroactive Shape Memory Performance of EVA/PCL/CNT Blend Composites with Selectively Localized CNTs, The Journal of Physical Chemistry C 120(40) (2016) 22793-22802. https://doi.org/10.1021/acs.jpcc.6b06345.
[151] D.H. Yi, H.J. Yoo, S.S. Mahapatra, Y.A. Kim, J.W. Cho, The synergistic effect of the combined thin multi-walled carbon nanotubes and reduced graphene oxides on photothermally actuated shape memory polyurethane composites, Journal of colloid and interface science 432 (2014) 128-134.
[152] Z. Wang, J. Zhao, M. Chen, M. Yang, L. Tang, Z.-M. Dang, F. Chen, M. Huang, X. Dong, Dually actuated triple shape memory polymers of cross-linked polycyclooctene–carbon nanotube/polyethylene nanocomposites, ACS applied materials & interfaces 6(22) (2014) 20051-20059.

[153] S. Wu, H. Luo, W. Shen, J. Su, C. Ma, J. Wu, Rapidly NIR-responsive electrospun shape memory actuators with MXene/CNCs hybrids, Materials Letters 314 (2022) 131922.
[154] J. Meng, J. Luo, H. Wang, Y. Quan, J. Li, X.J.C.C. Sun, Silver-decorated MXene nanosheets as a radical initiator for polymerization and multifunctional hydrogels, 58(48) (2022) 6821-6824.
[155] K. Yang, F. Yin, D. Xia, H. Peng, J. Yang, W.J.N. Yuan, A highly flexible and multifunctional strain sensor based on a network-structured MXene/polyurethane mat with ultra-high sensitivity and a broad sensing range, 11(20) (2019) 9949-9957.
[156] J.-H. Pu, X. Zhao, X.-J. Zha, L. Bai, K. Ke, R.-Y. Bao, Z.-Y. Liu, M.-B. Yang, W.J.J.o.M.C.A. Yang, Multilayer structured AgNW/WPU-MXene fiber strain sensors with ultrahigh sensitivity and a wide operating range for wearable monitoring and healthcare, 7(26) (2019) 15913-15923.
[157] Y.-w. Shao, W.-w. Hu, M.-h. Gao, Y.-y. Xiao, T. Huang, N. Zhang, J.-h. Yang, X.-d. Qi, Y.J.C.P.A.A.S. Wang, Manufacturing, Flexible MXene-coated melamine foam based phase change material composites for integrated solar-thermal energy conversion/storage, shape memory and thermal therapy functions, 143 (2021) 106291.
[158] W.-w. Hu, X.-y. Shi, M.-h. Gao, C.-h. Huang, T. Huang, N. Zhang, J.-h. Yang, X.-d. Qi, Y.J.C.C. Wang, Light-actuated shape memory and self-healing phase change composites supported by MXene/waterborne polyurethane aerogel for superior solar-thermal energy storage, 28 (2021) 100980.
[159] K. Li, T.H. Chang, Z. Li, H. Yang, F. Fu, T. Li, J.S. Ho, P.Y.J.A.E.M. Chen, Biomimetic MXene textures with enhanced light-to-heat conversion for solar steam generation and wearable thermal management, 9(34) (2019) 1901687.
[160] F. Javadi, H. Metselaar, P.J.S.E. Ganesan, Performance improvement of solar thermal systems integrated with phase change materials (PCM), a review, 206 (2020) 330-352.
[161] H. Gao, J. Wang, X. Chen, G. Wang, X. Huang, A. Li, W.J.N.E. Dong, Nanoconfinement effects on thermal properties of nanoporous shape-stabilized composite PCMs: A review, 53 (2018) 769-797.
[162] M.M. Umair, Y. Zhang, K. Iqbal, S. Zhang, B.J.A.e. Tang, Novel strategies and supporting materials applied to shape-stabilize organic phase change materials for thermal energy storage–A review, 235 (2019) 846-873.
[163] M. Subramanian, A.T. Hoang, B. Kalidasan, S. Nižetić, J.M. Solomon, D. Balasubramanian, C. Subramaniyan, G. Thenmozhi, H. Metghalchi, X.P.J.J.o.C.P. Nguyen, A technical review on composite phase change material based secondary assisted battery thermal management system for electric vehicles, 322 (2021) 129079.
[164] J. Yang, L.-S. Tang, L. Bai, R.-Y. Bao, Z.-Y. Liu, B.-H. Xie, M.-B. Yang, W.J.M.H. Yang, High-performance composite phase change materials for energy conversion based on macroscopically three-dimensional structural materials, 6(2) (2019) 250-273.
[165] J. Shi, M. Qin, W. Aftab, R.J.E.S.M. Zou, Flexible phase change materials for thermal energy storage, 41 (2021) 321-342.
[166] G. Li, X. Zhang, J. Wang, J.J.J.o.M.C.A. Fang, From anisotropic graphene aerogels to electron-and photo-driven phase change composites, 4(43) (2016) 17042-17049.
[167] R. Chen, R. Yao, W. Xia, R.J.A.E. Zou, Electro/photo to heat conversion system based on polyurethane embedded graphite foam, 152 (2015) 183-188.
[168] L. Chen, R. Zou, W. Xia, Z. Liu, Y. Shang, J. Zhu, Y. Wang, J. Lin, D. Xia, A.J.A.n. Cao, Electro-and photodriven phase change composites based on wax-infiltrated carbon nanotube sponges, 6(12) (2012) 10884-10892.
[169] X. Zhang, X. Wang, Z. Lei, L. Wang, M. Tian, S. Zhu, H. Xiao, X. Tang, L.J.A.a.m. Qu, interfaces, Flexible MXene-decorated fabric with interwoven conductive networks for integrated joule heating, electromagnetic interference shielding, and strain sensing performances, 12(12) (2020) 14459-14467.
[170] X. Fan, L. Liu, X. Jin, W. Wang, S. Zhang, B.J.J.o.M.C.A. Tang, MXene Ti 3 C 2 T x for phase change composite with superior photothermal storage capability, 7(23) (2019) 14319-14327.
[171] X. Lu, H. Huang, X. Zhang, P. Lin, J. Huang, X. Sheng, L. Zhang, J.-p. Qu, Novel light-driven and electro-driven polyethylene glycol/two-dimensional MXene form-stable phase change material with enhanced thermal conductivity and electrical conductivity for thermal energy storage, Composites Part B: Engineering 177 (2019) 107372. https://doi.org/https://doi.org/10.1016/j.compositesb.2019.107372.

[172] P. Lin, J. Xie, Y. He, X. Lu, W. Li, J. Fang, S. Yan, L. Zhang, X. Sheng, Y.J.S.E.M. Chen, S. Cells, MXene aerogel-based phase change materials toward solar energy conversion, 206 (2020) 110229.
[173] Z. Mo, P. Mo, M. Yi, Z. Hu, G. Tan, M.S. Selim, Y. Chen, X. Chen, Z. Hao, X. Wei, Ti3C2Tx@Polyvinyl alcohol foam-Supported Phase Change Materials with Simultaneous Enhanced Thermal Conductivity and Solar-Thermal Conversion Performance, Solar Energy Materials and Solar Cells 219 (2021) 110813. https://doi.org/https://doi.org/10.1016/j.solmat.2020.110813.
[174] V.K. Patle, Y. Mehta, N. Dwivedi, D.P. Mondal, A.K. Srivastava, R. Kumar, Thermal insulating and fire-retardant lightweight carbon-slag composite foams towards absorption dominated electromagnetic interference shielding, Sustainable Materials and Technologies 33 (2022) e00453. https://doi.org/https://doi.org/10.1016/j.susmat.2022.e00453.
[175] S. Chauhan, P. Nikhil Mohan, K.C.J. Raju, S. Ghotia, N. Dwivedi, C. Dhand, S. Singh, P. Kumar, Free-standing polymer/multiwalled carbon nanotubes composite thin films for high thermal conductivity and prominent EMI shielding, Colloids and Surfaces A: Physicochemical and Engineering Aspects 673 (2023) 131811. https://doi.org/https://doi.org/10.1016/j.colsurfa.2023.131811.
[176] A. Sharma, R. Kumar, A. Gupta, P.R. Agrawal, N. Dwivedi, D.P. Mondal, A.K. Srivastava, S.R. Dhakate, Enhanced electromagnetic interference shielding properties of phenolic resin derived lightweight carbon foam decorated with electrospun zinc oxide nanofibers, Materials Today Communications 30 (2022) 103055. https://doi.org/https://doi.org/10.1016/j.mtcomm.2021.103055.
[177] R. Kumar, A. Sharma, V.K. Patle, A. Pandey, N. Dwivedi, D.P. Mondal, Electromagnetic Interference Shielding in Phenolic Foam, in: S. P.K, S. M.S, S. Thomas (Eds.), Phenolic Based Foams: Preparation, Characterization, and Applications, Springer Nature Singapore, Singapore, 2022, pp. 175-193. https://doi.org/10.1007/978-981-16-5237-0_10.
[178] R. Kumar, A. Sharma, A. Pandey, A. Chaudhary, N. Dwivedi, M. Shafeeq M, D.P. Mondal, A.K. Srivastava, Lightweight carbon-red mud hybrid foam toward fire-resistant and efficient shield against electromagnetic interference, Scientific Reports 10(1) (2020) 9913. https://doi.org/10.1038/s41598-020-66929-3.
[179] W. Gao, N. Zhao, T. Yu, J. Xi, A. Mao, M. Yuan, H. Bai, C.J.C. Gao, High-efficiency electromagnetic interference shielding realized in nacre-mimetic graphene/polymer composite with extremely low graphene loading, 157 (2020) 570-577.
[180] F. Shahzad, M. Alhabeb, C.B. Hatter, B. Anasori, S. Man Hong, C.M. Koo, Y.J.S. Gogotsi, Electromagnetic interference shielding with 2D transition metal carbides (MXenes), 353(6304) (2016) 1137-1140.
[181] H. Duan, H. Zhu, J. Gao, D.-X. Yan, K. Dai, Y. Yang, G. Zhao, Y. Liu, Z.-M.J.J.o.M.C.A. Li, Asymmetric conductive polymer composite foam for absorption dominated ultra-efficient electromagnetic interference shielding with extremely low reflection characteristics, 8(18) (2020) 9146-9159.
[182] H. Xu, X. Yin, X. Li, M. Li, S. Liang, L. Zhang, L.J.A.a.m. Cheng, interfaces, Lightweight Ti2CT x MXene/poly (vinyl alcohol) composite foams for electromagnetic wave shielding with absorption-dominated feature, 11(10) (2019) 10198-10207.
[183] H. Liu, R. Fu, X. Su, B. Wu, H. Wang, Y. Xu, X.J.C.S. Liu, Technology, MXene confined in shape-stabilized phase change material combining enhanced electromagnetic interference shielding and thermal management capability, 210 (2021) 108835.
[184] W. Yuan, J. Yang, F. Yin, Y. Li, Y. Yuan, Flexible and stretchable MXene/Polyurethane fabrics with delicate wrinkle structure design for effective electromagnetic interference shielding at a dynamic stretching process, Composites Communications 19 (2020) 90-98. https://doi.org/https://doi.org/10.1016/j.coco.2020.03.003.
[185] X. Jia, B. Shen, L. Zhang, W.J.C.E.J. Zheng, Construction of shape-memory carbon foam composites for adjustable EMI shielding under self-fixable mechanical deformation, 405 (2021) 126927.
[186] X. Jia, B. Shen, L. Zhang, W.J.C. Zheng, Construction of compressible polymer/MXene composite foams for high-performance absorption-dominated electromagnetic shielding with ultra-low reflectivity, 173 (2021) 932-940.
[187] V. Salaris, A. Leonés, D. Lopez, J.M. Kenny, L. Peponi, Shape-memory materials via electrospinning: a review, Polymers 14(5) (2022) 995.

[188] D. Rokaya, H.E. Skallevold, V. Srimaneepong, A. Marya, P.K. Shah, Z. Khurshid, M.S. Zafar, J. Sapkota, Shape Memory Polymeric Materials for Biomedical Applications: An Update, Journal of Composites Science 7(1) (2023) 24.
[189] X. Yin, P. Tan, H. Luo, J. Lan, Y. Shi, Y. Zhang, H. Fan, L. Tan, Study on the release behaviors of berberine hydrochloride based on sandwich nanostructure and shape memory effect, Materials Science and Engineering: C 109 (2020) 110541.
[190] M. Bil, E. Kijeńska-Gawrońska, E. Głodkowska-Mrówka, A. Manda-Handzlik, P. Mrowka, Design and in vitro evaluation of electrospun shape memory polyurethanes for self-fitting tissue engineering grafts and drug delivery systems, Materials Science and Engineering: C 110 (2020) 110675.
[191] M. Bao, X. Wang, H. Yuan, X. Lou, Q. Zhao, Y. Zhang, HAp incorporated ultrafine polymeric fibers with shape memory effect for potential use in bone screw hole healing, Journal of Materials Chemistry B 4(31) (2016) 5308-5320.
[192] L.-F. Tseng, J. Wang, R.M. Baker, G. Wang, P.T. Mather, J.H. Henderson, Osteogenic capacity of human adipose-derived stem cells is preserved following triggering of shape memory scaffolds, Tissue Engineering Part A 22(15-16) (2016) 1026-1035.
[193] A. Lendlein, R. Langer, Biodegradable, elastic shape-memory polymers for potential biomedical applications, Science 296(5573) (2002) 1673-1676.
[194] F. Zhang, Z. Zhang, Y. Liu, W. Cheng, Y. Huang, J. Leng, Thermosetting epoxy reinforced shape memory composite microfiber membranes: Fabrication, structure and properties, Composites Part A: Applied Science and Manufacturing 76 (2015) 54-61.
[195] Z. Wu, L. Wei, S. Tang, Y. Xiong, X. Qin, J. Luo, J. Fang, X. Wang, Recent progress in Ti3C2T x MXene-based flexible pressure sensors, ACS nano 15(12) (2021) 18880-18894.
[196] N. Dwivedi, C. Dhand, P. Kumar, A. Srivastava, Emergent 2D materials for combating infectious diseases: The potential of MXenes and MXene–graphene composites to fight against pandemics, Materials Advances 2(9) (2021) 2892-2905.
[197] K. Huang, Z. Li, J. Lin, G. Han, P.J.C.S.R. Huang, Two-dimensional transition metal carbides and nitrides (MXenes) for biomedical applications, 47(14) (2018) 5109-5124.
[198] A. Liu, Y. Liu, G. Liu, A. Zhang, Y. Cheng, Y. Li, L. Zhang, L. Wang, H. Zhou, J. Liu, H. Wang, Engineering of surface modified Ti3C2Tx MXene based dually controlled drug release system for synergistic multitherapies of cancer, Chemical Engineering Journal 448 (2022) 137691. https://doi.org/https://doi.org/10.1016/j.cej.2022.137691.
[199] F. Mohajer, G.M. Ziarani, A. Badiei, S. Iravani, R.S.J.M. Varma, Advanced MXene-Based Micro-and Nanosystems for Targeted Drug Delivery in Cancer Therapy, 13(10) (2022) 1773.
[200] W.-J. Zhang, S. Li, V. Vijayan, J.S. Lee, S.S. Park, X. Cui, I. Chung, J. Lee, S.-k. Ahn, J.R.J.N. Kim, ROS-and pH-Responsive Polydopamine Functionalized Ti3C2Tx MXene-Based Nanoparticles as Drug Delivery Nanocarriers with High Antibacterial Activity, 12(24) (2022) 4392.
[201] C. Dai, H. Lin, G. Xu, Z. Liu, R. Wu, Y.J.C.o.M. Chen, Biocompatible 2D titanium carbide (MXenes) composite nanosheets for pH-responsive MRI-guided tumor hyperthermia, 29(20) (2017) 8637-8652.
[202] Z. Liu, M. Zhao, H. Lin, C. Dai, C. Ren, S. Zhang, W. Peng, Y.J.J.o.M.C.B. Chen, 2D magnetic titanium carbide MXene for cancer theranostics, 6(21) (2018) 3541-3548.
[203] X. Chang, Q. Wu, Y. Wu, X. Xi, J. Cao, H. Chu, Q. Liu, Y. Li, W. Wu, X.J.N.L. Fang, Multifunctional Au Modified Ti3C2-MXene for Photothermal/Enzyme Dynamic/Immune Synergistic Therapy, 22(20) (2022) 8321-8330.
[204] J. Yin, Q. Han, J. Zhang, Y. Liu, X. Gan, K. Xie, L. Xie, Y.J.A.a.m. Deng, interfaces, MXene-based hydrogels endow polyetheretherketone with effective osteogenicity and combined treatment of osteosarcoma and bacterial infection, 12(41) (2020) 45891-45903.
[205] C. Yang, Y. Luo, H. Lin, M. Ge, J. Shi, X.J.A.n. Zhang, Niobium carbide MXene augmented medical implant elicits bacterial infection elimination and tissue regeneration, 15(1) (2020) 1086-1099.
[206] S. Iravani, R.S.J.M.A. Varma, MXenes and MXene-based materials for tissue engineering and regenerative medicine: Recent advances, 2(9) (2021) 2906-2917.

[207] X. Mi, Z. Su, Y. Fu, S. Li, A.J.B.M. Mo, 3D printing of Ti3C2-MXene-incorporated composite scaffolds for accelerated bone regeneration, 17(3) (2022) 035002.
[208] S. Pan, J. Yin, L. Yu, C. Zhang, Y. Zhu, Y. Gao, Y.J.A.S. Chen, 2D MXene-integrated 3D-printing scaffolds for augmented osteosarcoma phototherapy and accelerated tissue reconstruction, 7(2) (2020) 1901511.
[209] G. Sun, X. Jiang, C. Liu, S. Song, J. Zhang, J. Shen, FeS@LAB-35@Ti3C2 as a high-efficiency nanozyme for near infrared light induced photothermal enhanced chemodynamic antibacterial activity and wound healing, Nano Research 16(2) (2023) 2840-2850. https://doi.org/10.1007/s12274-022-4965-3.
[210] C. Wischke, A.T. Neffe, S. Steuer, A.J.J.o.C.R. Lendlein, Evaluation of a degradable shape-memory polymer network as matrix for controlled drug release, 138(3) (2009) 243-250.
[211] M.C. Serrano, L. Carbajal, G.A.J.A.M. Ameer, Novel biodegradable shape-memory elastomers with drug-releasing capabilities, 23(19) (2011) 2211-2215.
[212] G. Li, G. Fei, H. Xia, J. Han, Y.J.J.o.m.c. Zhao, Spatial and temporal control of shape memory polymers and simultaneous drug release using high intensity focused ultrasound, 22(16) (2012) 7692-7696.
[213] H. Wache, D. Tartakowska, A. Hentrich, M.J.J.o.M.S.M.i.M. Wagner, Development of a polymer stent with shape memory effect as a drug delivery system, 14 (2003) 109-112.
[214] C.M. Yakacki, R. Shandas, C. Lanning, B. Rech, A. Eckstein, K.J.B. Gall, Unconstrained recovery characterization of shape-memory polymer networks for cardiovascular applications, 28(14) (2007) 2255-2263.
[215] W.M. Huang, C. Song, Y.Q. Fu, C.C. Wang, Y. Zhao, H. Purnawali, H. Lu, C. Tang, Z. Ding, J.J.A.D.D.R. Zhang, Shaping tissue with shape memory materials, 65(4) (2013) 515-535.
[216] M.-C. Chen, H.-W. Tsai, Y. Chang, W.-Y. Lai, F.-L. Mi, C.-T. Liu, H.-S. Wong, H.-W.J.B. Sung, Rapidly self-expandable polymeric stents with a shape-memory property, 8(9) (2007) 2774-2780.
[217] C.-S. Yang, H.-C. Wu, J.-S. Sun, H.-M. Hsiao, T.-W.J.A.a.m. Wang, interfaces, Thermo-induced shape-memory PEG-PCL copolymer as a dual-drug-eluting biodegradable stent, 5(21) (2013) 10985-10994.
[218] T. Gong, K. Zhao, W. Wang, H. Chen, L. Wang, S.J.J.o.M.C.B. Zhou, Thermally activated reversible shape switch of polymer particles, 2(39) (2014) 6855-6866.
[219] S.S. Sana, M. Santhamoorthy, R. Haldar, C.J. Raorane, S. Iravani, R.S. Varma, S.-C. Kim, Recent advances on MXene-based hydrogels for antibacterial and drug delivery applications, Process Biochemistry 132 (2023) 200-220. https://doi.org/https://doi.org/10.1016/j.procbio.2023.06.022.
[220] H. Li, R. Fan, B. Zou, J. Yan, Q. Shi, G. Guo, Roles of MXenes in biomedical applications: recent developments and prospects, Journal of Nanobiotechnology 21(1) (2023) 73. https://doi.org/10.1186/s12951-023-01809-2.
[221] T. Li, L. Chen, Y. Yuan, R. Shi, The Current Status, Prospects, and Challenges of Shape Memory Polymers Application in Bone Tissue Engineering, Polymers 15(3) (2023) 556.
[222] X. Zhai, Y. Ma, C. Hou, F. Gao, Y. Zhang, C. Ruan, H. Pan, W. Lu, W. Liu, 3D-Printed High Strength Bioactive Supramolecular Polymer/Clay Nanocomposite Hydrogel Scaffold for Bone Regeneration. ACS Biomater Sci Eng, 3: 1109–18, 2017.
[223] C. Dhand, N. Dwivedi, H. Sriram, S. Bairagi, D. Rana, R. Lakshminarayanan, M. Ramalingam, S. Ramakrishna, 8 - Nanofiber composites in drug delivery, in: M. Ramalingam, S. Ramakrishna (Eds.), Nanofiber Composites for Biomedical Applications, Woodhead Publishing2017, pp. 199-223. https://doi.org/https://doi.org/10.1016/B978-0-08-100173-8.00008-9.
[224] D. Zhang, O.J. George, K.M. Petersen, A.C. Jimenez-Vergara, M.S. Hahn, M.A.J.A.b. Grunlan, A bioactive "self-fitting" shape memory polymer scaffold with potential to treat cranio-maxillo facial bone defects, 10(11) (2014) 4597-4605.
[225] Y.-J. Wang, U.-S. Jeng, S.-h.J.A.B.S. Hsu, Engineering, Biodegradable water-based polyurethane shape memory elastomers for bone tissue engineering, 4(4) (2018) 1397-1406.
[226] H. Xuan, H. Hu, C. Geng, J. Song, Y. Shen, D. Lei, Q. Guan, S. Zhao, Z.J.A.B. You, Biofunctionalized chondrogenic shape-memory ternary scaffolds for efficient cell-free cartilage regeneration, 105 (2020) 97-110.
[227] S. Iravani, R.S. Varma, MXenes and MXene-based materials for tissue engineering and regenerative medicine: Recent advances, Materials Advances 2(9) (2021) 2906-2917.

[228] K. Chen, Y. Chen, Q. Deng, S.-H. Jeong, T.-S. Jang, S. Du, H.-E. Kim, Q. Huang, C.-M.J.M.L. Han, Strong and biocompatible poly (lactic acid) membrane enhanced by Ti3C2Tz (MXene) nanosheets for Guided bone regeneration, 229 (2018) 114-117.
[229] M. Li, J. Chen, M. Shi, H. Zhang, P.X. Ma, B.J.C.E.J. Guo, Electroactive anti-oxidant polyurethane elastomers with shape memory property as non-adherent wound dressing to enhance wound healing, 375 (2019) 121999.
[230] X. Zhao, B. Guo, H. Wu, Y. Liang, P.X.J.N.c. Ma, Injectable antibacterial conductive nanocomposite cryogels with rapid shape recovery for noncompressible hemorrhage and wound healing, 9(1) (2018) 2784.
[231] X. Xu, S. Wang, H. Wu, Y. Liu, F. Xu, J. Zhao, A multimodal antimicrobial platform based on MXene for treatment of wound infection, Colloids and Surfaces B: Biointerfaces 207 (2021) 111979. https://doi.org/https://doi.org/10.1016/j.colsurfb.2021.111979.
[232] D. Xu, Z. Li, L. Li, J. Wang, Insights into the photothermal conversion of 2D MXene nanomaterials: synthesis, mechanism, and applications, Advanced Functional Materials 30(47) (2020) 2000712.
[233] Z. Zhang, Z. Qi, W. Kong, R. Zhang, C. Yao, Applications of MXene and its modified materials in skin wound repair, Frontiers in Bioengineering and Biotechnology 11 (2023) 1154301.
[234] S. Liu, D. Li, Y. Wang, G. Zhou, K. Ge, L. Jiang, D. Fang, Flexible, high-strength and multifunctional polyvinyl alcohol/MXene/polyaniline hydrogel enhancing skin wound healing, Biomaterials Science 10(13) (2022) 3585-3596.
[235] Z. Wu, S. Li, X. Qin, L. Zheng, J. Fang, L. Wei, C. Xu, Z.A. Li, X. Wang, Facile preparation of fatigue-resistant Mxene-reinforced chitosan cryogel for accelerated hemostasis and wound healing, Carbohydrate Polymers 334 (2024) 121934.
[236] H.-J. Huang, Y.-L. Tsai, S.-H. Lin, S.-h. Hsu, Smart polymers for cell therapy and precision medicine, Journal of Biomedical Science 26(1) (2019) 73. https://doi.org/10.1186/s12929-019-0571-4.
[237] W. Feng, R. Wang, Y. Zhou, L. Ding, X. Gao, B. Zhou, P. Hu, Y.J.A.F.M. Chen, Ultrathin molybdenum carbide MXene with fast biodegradability for highly efficient theory-oriented photonic tumor hyperthermia, 29(22) (2019) 1901942.
[238] X. Han, J. Huang, H. Lin, Z. Wang, P. Li, Y.J.A.h.m. Chen, 2D ultrathin MXene-based drug-delivery nanoplatform for synergistic photothermal ablation and chemotherapy of cancer, 7(9) (2018) 1701394.
[239] A. Bhat, S. Anwer, K.S. Bhat, M.I.H. Mohideen, K. Liao, A. Qurashi, Prospects challenges and stability of 2D MXenes for clean energy conversion and storage applications, npj 2D Materials and Applications 5(1) (2021) 61. https://doi.org/10.1038/s41699-021-00239-8.
[240] S. Karamat, M. Kashif, S. Anwar, U. Batool, M. Talha, U. Khalique, M.M. Rahman, Unveiling the Latest Advancements in Vanadium Carbide MXene based Supercapacitors and their Future Trends, Chemistry–An Asian Journal 19(2) (2024) e202300919.
[241] S. Venkateshalu, J. Cherusseri, M. Karnan, K.S. Kumar, P. Kollu, M. Sathish, J. Thomas, S.K. Jeong, A.N. Grace, New method for the synthesis of 2D vanadium nitride (MXene) and its application as a supercapacitor electrode, ACS omega 5(29) (2020) 17983-17992.
[242] G. Guan, F. Guo, A Review of Nb2CTx MXene: Synthesis, Properties and Applications, Batteries 9(4) (2023) 235.
[243] N. Bisht, M. Patel, D. Mondal, A.K. Srivastava, N. Dwivedi, C. Dhand, Comparative performance analysis of mussel-inspired polydopamine, polynorepinephrine, and poly-α-methyl norepinephrine in electrochemical biosensors, Microchimica Acta 191(8) (2024) 456.
[244] M. Pandey, K. Deshmukh, A. Raman, A. Asok, S. Appukuttan, G.R. Suman, Prospects of MXene and graphene for energy storage and conversion, Renewable and Sustainable Energy Reviews 189 (2024) 114030. https://doi.org/https://doi.org/10.1016/j.rser.2023.114030.
[245] Z. Zhu, An Overview of Carbon Nanotubes and Graphene for Biosensing Applications, Nano-Micro Letters 9(3) (2017) 25. https://doi.org/10.1007/s40820-017-0128-6.
[246] J. Liu, X. Jia, Y. Liu, Y. Wuliu, J. Dai, X. Zhu, X. Liu, A synergetic strategy of well dispersing hydrophilic Ti3C2Tx MXene into hydrophobic polybenzoxazine composites for improved comprehensive performances, Composites Science and Technology 219 (2022) 109248. https://doi.org/https://doi.org/10.1016/j.compscitech.2021.109248.

[247] H.T.A. Awan, M.A.A.M. Abdah, M. Mehar, R. Walvekar, V. Chaudhary, M. Khalid, A. Khosla, MXene-polymer hybrid composites for advanced energy storage: Insights into supercapacitors and batteries, Journal of Energy Storage 95 (2024) 112449. https://doi.org/https://doi.org/10.1016/j.est.2024.112449.
[248] K. Wang, L. Shen, Q. Zhu, R. Bo, R. Lu, X. Lu, Z. Fu, Construction of modified MXene with "organic–inorganic" structure to enhance the interfacial and mechanical properties of UHMWPE fiber-reinforced epoxy composite, Chemical Engineering Journal 452 (2023) 139156.
[249] Y. Sliozberg, J. Andzelm, C.B. Hatter, B. Anasori, Y. Gogotsi, A. Hall, Interface binding and mechanical properties of MXene-epoxy nanocomposites, Composites Science and Technology 192 (2020) 108124.
[250] D. Wang, H. Wei, Y. Lin, P. Jiang, H. Bao, X. Huang, Achieving ultrahigh thermal conductivity in Ag/MXene/epoxy nanocomposites via filler-filler interface engineering, Composites Science and Technology 213 (2021) 108953.
[251] A. Liang, X. Jiang, X. Hong, Y. Jiang, Z. Shao, D. Zhu, Recent Developments Concerning the Dispersion Methods and Mechanisms of Graphene, Coatings 8(1) (2018) 33.
[252] Z. Ling, C.E. Ren, M.-Q. Zhao, J. Yang, J.M. Giammarco, J. Qiu, M.W. Barsoum, Y. Gogotsi, Flexible and conductive MXene films and nanocomposites with high capacitance, Proceedings of the National Academy of Sciences 111(47) (2014) 16676-16681.
[253] J. Ji, L. Zhao, Y. Shen, S. Liu, Y. Zhang, Covalent stabilization and functionalization of MXene via silylation reactions with improved surface properties, FlatChem 17 (2019) 100128. https://doi.org/https://doi.org/10.1016/j.flatc.2019.100128.
[254] C. Chen, M. Boota, X. Xie, M. Zhao, B. Anasori, C.E. Ren, L. Miao, J. Jiang, Y. Gogotsi, Charge transfer induced polymerization of EDOT confined between 2D titanium carbide layers, Journal of Materials Chemistry A 5(11) (2017) 5260-5265.
[255] R. Liu, W. Li, High-thermal-stability and high-thermal-conductivity Ti3C2T x MXene/poly (vinyl alcohol)(PVA) composites, ACS omega 3(3) (2018) 2609-2617.
[256] H. Riazi, M. Anayee, K. Hantanasirisakul, A.A. Shamsabadi, B. Anasori, Y. Gogotsi, M. Soroush, Surface modification of a MXene by an aminosilane coupling agent, Advanced Materials Interfaces 7(6) (2020) 1902008.
[257] T. Li, B. Ding, J. Wang, Z. Qin, J.F. Fernando, Y. Bando, A.K. Nanjundan, Y.V. Kaneti, D. Golberg, Y. Yamauchi, Sandwich-structured ordered mesoporous polydopamine/MXene hybrids as high-performance anodes for lithium-ion batteries, ACS applied materials & interfaces 12(13) (2020) 14993-15001.
[258] G.S. Lee, T. Yun, H. Kim, I.H. Kim, J. Choi, S.H. Lee, H.J. Lee, H.S. Hwang, J.G. Kim, D.-w. Kim, Mussel inspired highly aligned Ti3C2T x MXene film with synergistic enhancement of mechanical strength and ambient stability, ACS nano 14(9) (2020) 11722-11732.
[259] X. Liu, Y. Liu, S. Dong, X. Zhang, S. Hou, Synthesis of ultra-high specific surface area aerogels with nitrogen-enriched Ti 3 C 2 T x nanosheets as high-performance supercapacitor electrodes, Journal of Materials Chemistry C 10(40) (2022) 14929-14938.